OFFICE OF NAVAL RESEARCH

Grant No.

R&T Code N00014-92-C-0173

Technical Report #01

ADSORPTION OF HYDRATED HALIDE IONS ON CHARGED ELECTRODES. MOLECULAR DYNAMICS SIMULATION.

by

James N. Glosli
Michael R. Philpott

Prepared for publication

in the

Journal of Chemical Physics

IBM Research Division, Almaden Research Center,
650 Harry Road, San Jose, CA 95120-6099

1993

SECURITY CLASSIFICATION OF THIS PAGE *(When Data Entered)*

REPORT DOCUMENTATION PAGE		READ INSTRUCTIONS BEFORE COMPLETING FORM
1. REPORT NUMBER 01	2 GOVT ACCESSION NO	3 RECIPIENT'S CATALOG NUMBER
Technical Report 16 4. TITLE *(and Subtitle)* Adsorption of Hydrated Halide Ions on Charged Electrodes. Molecular Dynamics Simulation.		5 TYPE OF REPORT & PERIOD COVERED Technical Report 6 PERFORMING ORG REPORT NUMBER
7. AUTHOR(s) James N. Glosli Michael R. Philpott		8 CONTRACT OR GRANT NUMBER(s) N00014-92-C-0173
9 PERFORMING ORGANIZATION NAME AND ADDRESS IBM Research Division, Almaden Research Center 650 Harry Road San Jose, CA 95120-6099		10 PROGRAM ELEMENT, PROJECT, TASK AREA & WORK UNIT NUMEERS
11. CONTROLLING OFFICE NAME AND ADDRESS Office of Naval Research 800 North Quincy Street Arlington, VA 22217		12 REPORT DATE 4/14/93 13 NUMBER OF PAGES 57
14. MONITORING AGENCY NAME & ADDRESS *(If different from Controlling Office)* Dr. Ronald A. De Marco Office of Naval Research, Chemistry Division 800 N. Quincy Street Arlington, VA 22217 U.S.A.		15 SECURITY CLASS *(of this report)* Unclassified 15a DECLASSIFICATION/DOWNGRADING SCHEDULE

16. DISTRIBUTION STATEMENT *(of this Report)*
Approved for public release; unlimited distribution.

17. DISTRIBUTION STATEMENT *(of the abstract entered in Block 20, if different from Report)*
Approved for public release; unlimited distribution.

18. SUPPLEMENTARY NOTES
Prepared for publication in Journal of Chemical Physics (1993)

19. KEY WORDS *(Continue on reverse side if necessary and identify by block number)*

20 ABSTRACT *(Continue on reverse side if necessary and identify by block number)*
SEE NEXT PAGE

SECURITY CLASSIFICATION OF THIS PAGE *(When Data Entered)*

Constant temperature molecular dynamics has been used to simulate the adsorption of hydrated halide ions X^- = F^-, Cl^-, Br^- and I^-, and lithium ion Li^+ on a flat uniformly charged surfaces. The simulations were done with either 214 water molecules and two ions (Li^+ and X^-) in a box 2.362 nm deep or with 430 water molecules and the two ions in a box 4.320 nm deep. The boxes were periodically replicated in the xy directions. The magnitude of the surface charge on the box ends was ± 0.11 e/(nm)^2, corresponding to an electric field of 2×10^7 V/cm. The lateral dimensions of the simulation cell were 1.862 nm × 1.862 nm (x × y) in each case. All of the water molecules and ions interacted with the end walls via a weak 9 - 3 potential. The ST2 water model and parameters optimized for alkali halides interacting with the model ST2 water molecule were used in the calculations. Common practices of truncating the interactions at a finite distance (0.82 nm) and switching off Coulomb interactions at small distances were followed. The temperature was set at T = 2.411 kJ/mole (290 K).

Some of the properties calculated were: distribution density profiles for ions and water across the gap important for comparisons with Gouy-Chapman theory, adsorbed ion - water pair correlation functions, the number of water molecules in the first and second hydration shells of the ions as a function of time. The time spent by a water molecule in the hydration shell was calculated to be approximately ten times longer for lithium than any other ion. The correlation between distance from the electrode and hydration number was studied and generally found to be pronounced for the larger anions. Comparison of the dynamics of the common ion Li^+ for different anions revealed the subtle influence of a transcell interaction in the 2.362 nm thick film.

In the given field the smallest ions Li^+ and F^- remained fully solvated at all times. Chloride behaved quite differently. Part of the time this ion was far enough away from the electrode to be fully hydrated and part of the time it was in physical contact (ie., physisorbed) on the electrode with no water molecules interposed between it and the electrode. Bromide favoured contact adsorption over full hydration most of the time. Iodide was observed to be contact adsorbed almost all of the time. These simulations provide new insights on the behavior of strongly hydrated ions at surfaces and how the transition from non-contact to 'contact' adsorption occurs.

ADSORPTION OF HYDRATED HALIDE IONS ON CHARGED ELECTRODES. MOLECULAR DYNAMICS SIMULATION.

James N. Glosli
and
Michael R. Philpott

IBM Research Division
Almaden Research Center
650 Harry Road
San Jose, CA 95120-6099

ABSTRACT

Constant temperature molecular dynamics has been used to simulate the adsorption of hydrated halide ions X^- = F^-, Cl^-, Br^- and I^-, and lithium ion Li^+ on a flat uniformly charged surfaces. The simulations were done with either 214 water molecules and two ions (Li^+ and X^-) in a box 2.362 nm deep or with 430 water molecules and the two ions in a box 4.320 nm deep. The boxes were periodically replicated in the xy directions. The magnitude of the surface charge on the box ends was ± 0.11 c/(nm)^2, corresponding to an electric field of 2×10^7 V/cm. The lateral dimensions of the simulation cell were 1.862 nm × 1.862 nm (x × y) in each case. All of the water molecules and ions interacted with the end walls via a weak 9 - 3 potential. The ST2 water model and parameters optimized for alkali halides interacting with the model ST2 water molecule were used in the calculations. Common practices of truncating the interactions at a finite distance (0.82 nm) and switching off Coulomb interactions at small distances were followed. The temperature was set at T = 2.411 kJ/mole (290 K).

Some of the properties calculated were: distribution density profiles for ions and water across the gap important for comparisons with Gouy-Chapman theory, adsorbed ion - water pair correlation functions, the number of water molecules in the first and second hydration shells of the ions as a function of time. The time spent by a water molecule in the hydration shell was calculated to be approximately ten times longer for lithium than any other ion. The correlation between distance from the electrode and hydration number was studied and generally found to be pronounced for the larger anions. Comparison of the dynamics of the common ion Li^+ for different anions revealed the subtle influence of a transcell interaction in the 2.362 nm thick film.

In the given field the smallest ions Li^+ and F^- remained fully solvated at all times. Chloride behaved quite differently. Part of the time this ion was far enough away from the electrode to be fully hydrated and part of the time it was in physical contact (ie., physisorbed) on the

electrode with no water molecules interposed between it and the electrode. Bromide favoured contact adsorption over full hydration most of the time. Iodide was observed to be contact adsorbed almost all of the time. These simulations provide new insights on the behavior of strongly hydrated ions at surfaces and how the transition from non-contact to 'contact' adsorption occurs.

I.INTRODUCTION

In a previous paper (1), constant energy molecular dynamics simulations of the adsorption lithium and iodide ions from aqueous solution onto charged surfaces were described. This paper continues this study with an investigation of the halide series (fluoride, chloride, bromide, and iodide) characterized by increasing ionic radius and decreasing hydration enthalpies, adsorbed on an idealized flat charged surface situated at the ends of a box replicated periodically in the lateral (xy) directions.

Capacitance, chronocoulombic, spectroscopic and ellipsometric measurements of ions adsorbed at electrochmeical interfaces have long been interpreted using a standardized model (2-4). It has been shown that the larger ions adsorb with at least partial loss of the inner solvation shell. For metal electrodes this process is called contact adsorption, and on some noble metals a series has been determined in which higher members displace lower ones from the surface (2, 5). A fuller discussion was given in the first paper (1). It is a goal of this paper to understand more about the transition from adsorbed but fully solvated ion to adsorbed ion in physical contact with the surface when there is a static electric field attracting the ion to the surface. We tacitly assume this local property of the ions is not greatly affected by gross misshandling of the long range electrostatic fields of the interface through the application of the cut-off. The field chosen is at the upper end of fields in thermodynamically stable double layers. In weaker fields the average position of the ion was closer to film center (6). We show how essential features of the contacting process can be modeled with a system consisting of two ions and 214 water molecules sandwiched between charged nonmetallic plates 2.362 nm apart. More elaborate calculations with 430 waters, two ions and plates 4.320 nm apart were performed to check for transcell interactions between adsorbed ions. Such interactions were indeed found. The study revealed new features about the way the adsorption process proceeds. Properties calculated and reported here include: time dependence of the z

coordinates of ions, time dependence of ion hydration numbers, time averaged distribution of ions and water across the electrolyte film, and the ion-water pair correlation functions. The first property showed that the transition to contract adsorption first occurs for Cl^- in the given electric field. The second showed how solvation shells were affected as the adsorbed ions jittered back and forth under opposing influences of thermal forces and the combined attraction of the electric and wall forces.

All the frequently used water models (ST2, TIPS and SPCE) (7-9), have parameters optimized to bulk properties. Consequently none may be adequate to describe quantitatively a water molecule outside a mean field approximation to it's bulk environment. Our strategy to side step this difficulty is to perform calculations on a series of related ions in the expectation that by considering a series with the same charge and a graduated property like radius, the water-ion-wall interactions will span the experimental range of phenomena observed as ions approach a charged surface. The presence of the Li^+ counter ion in all the calculations provides a useful sanity check against pathological conditions that might arise due to the assumptions like finite cut-off of long range interactions. With the exception of Xe-Pt(111) system (10) there are no well proven or tested molecule- or ion-surface potentials. Consequently we are currently unable to connect directly with either ex situ measurements e.g., I^- on Pt(111) or Cl^- on Ag(100) performed by transferring emersed electrodes into UHV (11) or in situ surface crystallographic measurements like Sexafs and Xanes of under potentially deposited (upd) metals (12, 13).

In one respect the model used here was simpler than the set of assumptions constituting the standard model (2) of ionic adsorption on metal electrodes. In our model all species were attracted to the electrodes by the same 'wall' potential. This potential and the static electric field were not subject to the 0.82 nm cut-off applied to all the intermolecular interactions.

The ST2 parameters describing lithium and to a lesser extent fluoride are suspect because in the case of lithium ion the hydration enthalpy calculated is too large compared to experiment (14-16). It is possible that the adsorption of the smallest ions Li^+ and F^- as fully hydrated species in the $2x10^7$ V/cm field could be artifacts due to the exaggerated hydration enthalpy. However this argument does not affect our general conclusions if only because the applied static field used is at the upper end of fields encountered in electrochemical double layers and if more realistic model parameters had weaker hydration interactions there would still be fields where the small ions would adsorb fully hydrated. In weaker fields than the one used in this paper the ions relax towards film center (6). We will discuss the effect this could have on the interpretation of the calculations more fully in a later section.

Another point of concern is the electrical discharge of contact adsorbed ions. In the older papers and text books (2, 17) halide adsorption is treated as a physisorption phenomenon. However there is exceptionaly good experimental evidence that argues strongly that this is far too simplistic a picture. After contact adsorption a large polarizable ions like iodide on metals Au and Pt can 'discharge' and become chemisorbed (11, 18-21). Discharge of ions and the formation of chemisorbed species is outside the scope of the classical molecular dynamics scheme used here. tains its full charge.

We close this section with a brief review of recent MD calculations in the general area of solid - aqueous interfaces. In a very early study, the Mainz group (22, 23), followed the evolution of eight LiI and 200 water molecules between Lennard - Jones walls for 10 and 20 ps. They were only able to calculate short time correlation functions and not the adsorption process which required a longer simulation than they were able to do at the time. Rose and Benjamin (24) have described MD simulations of a single Na^+ and a single Cl^- ion in a slab of 512 waters (flexible SPC model (25),) between two Pt(100) surfaces. The geometry and potentials were those devised

by Heinzinger and coworkers (26, 27). For Pt(100) the first monolayer of water was strongly bound. A result of significance was the calculation of the Helmholtz free energy of adsorption in zero electric field. The anion was more strongly bound than the cation. More recently Seitz-Beywl et al (28) have studied hydration of Li^+ and I^- separately in three layers of water at the Pt surface. They used the flexible water model of Bopp et al (29), in a simulation lasting 7.5 ps. The work reported here is complementary to that cited and described above.

There is also continuing interest in thin films of water and electrolytes in connection with a possible phase transition (30, 31), vibrational relaxation dynamics, hydrogen bond formation dynamics (32, 33), and the interaction of water with metals treated as jellium half spaces (34).

This paper is arranged as follows. Section II describes the models used for ions and water and details of computation. Sections III through VII describe the results for the halide ions, and the last section summarizes the main results and conclusions for this series of simulations.

II. THE MODEL

In the calculations described here we use the water model originally devised by Stillinger (7, 35), and commonly referred to as the ST2 model. Although this model required more computer time because it contains four charged and one uncharged point particles, this draw back is more than compensated by the extensive set of Lennard-Jones parameters for use with all the alkali metal cations and halide anions. These parameters were developed in a series of molecular dynamics calculations by Heinzinger and Spohr (26, 27).

Interaction Energy

The Coulomb interaction between molecules was represented as sum of $1/r$ interactions between atomic point charges. These interactions were soften for small molecular separation by a switching function $S(R)$. This switching function was introduced by Stillinger (7), and was clearly documented by Steinhauser (35). The short range part of the intermolecular interaction was modeled by Lennard-Jones potential between the atoms of each molecule. All molecule-molecule interactions (both $1/r$ and Lennard-Jones potentials) were cut-off in a smooth fashion at molecular separation $R = 0.82$ nm by a truncation function $T(R)$. The atoms of each molecule also interacted with surfaces at $z = \pm z_o$. Both surfaces were treated as flat featureless plates with a uniform electric charge density of $+\sigma$ and $-\sigma$ on the $-z_o$ and $+z_o$ plates respectively. This gave rise to a uniform electric field, $E = 4\pi K\sigma$ in the positive z-direction where the electrostatic coupling constant K had the value 138.936 KJ•nm/(mole• e^2) in the units used in this calculation. Non Coulombic interactions between the walls and all the atoms were represented by the 9-3 potential (wall potential) introduced by Lee et al (36). The complete interaction energy U is,

$$U = \sum_{\substack{\alpha \in A_i \\ \beta \in A_j \\ i<j}} \left\{ \frac{K q_\alpha q_\beta}{r_{\alpha\beta}} S(R_{ij}, R_L^{ij}, R_U^{ij}) + 4\varepsilon_{\alpha\beta} \left[\left(\frac{\sigma_{\alpha\beta}}{r_{\alpha\beta}} \right)^{12} - \left(\frac{\sigma_{\alpha\beta}}{r_{\alpha\beta}} \right)^{6} \right] \right\} T(R_{ij}) \tag{1}$$

$$+ \sum_{\alpha} \left\{ - q_\alpha E z_\alpha + \left(\frac{A_\alpha}{(z_\alpha + z_O)^9} - \frac{B_\alpha}{(z_\alpha + z_O)^3} \right) + \left(\frac{A_\alpha}{(z_\alpha - z_O)^9} - \frac{B_\alpha}{(z_\alpha - z_O)^3} \right) \right\}$$

where i and j were molecular indices, and, α and β were atomic indices. Here A_i was the set of all atoms of molecule i , R_{ij} was the distance between the center of mass of molecules i and j, and The symbol $r_{\alpha\beta}$ was the distance between atoms α and β. For small R the Coulomb energy was modified by the switching function $S(R, R_L, R_U)$ given by,

$$S(R, R_L, R_U) = \begin{cases} 0 & R < R_L \\ \dfrac{(R - R_L)^2 (3R_U - 2R - R_L)}{(R_U - R_L)^3} & R_L < R < R_U \\ 1 & R_U < R \end{cases} \tag{2}$$

The values of R_L and R_U were dependent on the types of the molecular species that were interacting.

As mentioned above the tails of Coulomb and Lennard-Jones pair interactions were cut off by the truncation function $T(R)$. The form of $T(R)$ was given by,

$$T(R) = \begin{cases} 1 & R < R_L^T \\ \left(1 - \left(\dfrac{R - R_L^T}{R_U^T - R_L^T} \right)^m \right)^n & R_L^T < R < R_U^T \\ 0 & R_U^T < R \end{cases} \qquad (3)$$

The same truncation function was applied to all molecular interactions, with $R_L^T = 0.779$ nm and $R_U^T = 0.820$ nm. The integers m and n controlled the smoothness of the truncation function at R_L^T and R_U^T respectively. In these calculations $n = m = 2$ which insured that the energy had smooth first spatial derivatives.

Equations of motion

All molecules, in this study, were considered as a rigid collection of point atoms. That is all bond lengths and angles within a molecule were fixed. To evolve a collection of these molecules a quaternion formulation of the rigid body equations of motion was used (37). The center of mass position ($\mathbf{R}_i$) and velocity ($\mathbf{V}_i$) was used to describe the translational degrees of freedoms of molecule i. The orientational motion of the molecule was described by the quaternion $\mathbf{q}_i = (q_i^0, q_i^1, q_i^2, q_i^3)$ and the rotational velocity ($\boldsymbol{\omega}_i^b$), as measured in the body frame of the molecule. The one exception to this was for monatomic molecules, in which case the orientational degrees of freedom were not needed.

The discussion of the equations of motion begin by considering the potential energy U. From equation 1, it can be seen that the potential energy can be treated as a scalar function of the variables ($\mathbf{R}_1,\ldots, \mathbf{R}_N; \mathbf{r}_1,\ldots, \mathbf{r}_n$), where N is the number of molecules and n is the number of atoms in the entire system.

$$U = U(\mathbf{R}_1,\ldots, \mathbf{R}_N; \mathbf{r}_1,\ldots, \mathbf{r}_n) \qquad (4)$$

Of course not all these variables are independent. However for the purposes of the following two definitions they are treated as independent variables.

$$\mathbf{f}_\alpha \equiv \nabla_{\mathbf{r}_\alpha} U, \qquad \mathbf{F}_i \equiv \nabla_{\mathbf{R}_i} U. \tag{5}$$

The total force $\mathbf{F}_i^T$ and torque $\boldsymbol{\tau}_i$ can be expressed in terms of $\mathbf{f}_\alpha$ and $\mathbf{F}_i$ as

$$\mathbf{F}_i^T = \mathbf{F}_i + \sum_{\alpha \in A_i} \mathbf{f}_\alpha \qquad \boldsymbol{\tau}_i = \sum_{\alpha \in A_i} (\mathbf{r}_\alpha - \mathbf{R}_i) \times \mathbf{f}_\alpha, \tag{6}$$

The translational motion of the molecule is described by the first order ordinary differential equation,

$$\frac{d\mathbf{R}_i}{dt} = \mathbf{V}_i \qquad M_i \frac{d\mathbf{V}_i}{dt} = \mathbf{F}_i^T. \tag{7}$$

For the rotational motion it is convenient to work in the body axis of the molecule, where the moment of inertia $\hat{I}_i$ is diagonal and time independent. It is useful to define the operator $\hat{Q}_i$

$$\hat{Q}_i = \begin{bmatrix} -q_i^1 & -q_i^2 & -q_i^3 \\ q_i^0 & -q_i^3 & q_i^2 \\ q_i^3 & q_i^0 & -q_i^1 \\ -q_i^2 & q_i^1 & q_i^0 \end{bmatrix} \tag{8}$$

and the body frame rotational force

$$\mathbf{F}_i^R = \boldsymbol{\tau}_i^b - \boldsymbol{\omega}_i^b \times (\hat{I}_i^b \boldsymbol{\omega}_i^b). \tag{9}$$

Using these quantities above, the following first order ordinary differential equations can be written to describe the rotational motion

$$\frac{d\mathbf{q}_i}{dt} = \hat{Q}_i \boldsymbol{\omega}_i^b \qquad \hat{I}_i^b \frac{d\boldsymbol{\omega}_i^b}{dt} = \mathbf{F}_i^R. \tag{10}$$

This set of equations conserve the total energy for time independent potentials (U) . A constant temperature ensemble may be simulated by introducing a velocity dependent term in the acceleration terms to constrain the total kinetic energy. The constant temperature equations of motion are written as,

$$\frac{d\mathbf{R}_i}{dt} = \mathbf{V}_i, \qquad M_i \frac{d\mathbf{V}_i}{dt} = \mathbf{F}_i^T - \gamma \mathbf{V}_i$$

$$\frac{d\mathbf{q}_i}{dt} = \hat{Q}_i \boldsymbol{\omega}_i^b, \qquad (\hat{I}_i)^b \frac{d\boldsymbol{\omega}_i^b}{dt} = \mathbf{F}_i^R - \gamma \boldsymbol{\omega}_i^b. \tag{11}$$

$$\gamma = \left(\sum_i \mathbf{V}_i \mathbf{F}_i^T + \boldsymbol{\omega}_i^b \mathbf{F}_i^b\right)/(2K)$$

This choice of γ ensures that the total kinetic energy of the systems is constant.

Model for water molecules and ions.

In the ST2 model the water molecule consisted of a central oxygen atom (O_ST2) surrounded by two hydrogen atoms (H_ST2) and two massless point charges (PC_ST2) in a rigid tetrahedral arrangement (bond angle = $\cos^{-1}(1/\sqrt{3})$). The O_ST2/H_ST2 and O_ST2/PC_ST2 bond lengths were 0.10 nm and 0.08 nm respectively. The oxygen atom was the only Lennard-Jones 'atom' in ST2 water. The hydrogen and point charges interacted with their surroundings (i.e. atoms and surfaces) by Coulomb interactions only. The ions were treated as non polarizable Lennard-Jones 'atom' with point mass and charge.

Interaction Parameters.

The atom-atom and atom-surface interaction parameters are given in Table I. These parameters are taken from work of Heinzinger and Spohr (26, 27). The combining

rules for unlike species were: $\varepsilon_{AB} = (\varepsilon_{AA}\varepsilon_{BB})^{1/2}$, $\sigma_{AB} = \frac{1}{2}(\sigma_{AA} + \sigma_{BB})$. The switching function interval ends R_l^{η} and R_u^{η} all vanish except for ST2/ST2 pairs, where $R_L^{ST2,ST2} = 0.20160$ nm and $R_U^{ST2,ST2} = 0.31287$ nm.

Simulation details

The systems considered had either 216 or 432 molecules and ions. In the main set of simulations a system of 214 water ST2 molecules, one Li ion and one halide ion were studied. For all systems the molecules were confined to a rectangular simulation box with dimensions 1.862 nm × 1.862 nm ×2.362 nm (x × y × z) and periodic boundary conditions in the x and y directions. In the calculations with 432 molecules the simulation box had the same x and y dimensions and was 4.230 nm thick in the z direction. Initially the molecules were randomly disposed on a cubic lattice with lattice parameter 0.31 nm. The equations of motion were integrated by a fourth order multi-step numerical scheme with a 2 fs time step. With this scheme the time step to time step rms fluctuation of quaternions length and energy/temperature was about 0.0002% and 0.0009%/0.002% respectively. Though small, these changes could lead to global drift, so at each time step a small scaling correction was made to the quaternions and velocities. Also the global center of mass velocities in the x and y directions was set to zero at each time step by shifting the molecular translational velocities

All calculations were performed on an IBM RS/6000 model 540 operating at 16 Mflop. For the simulations involving 432 molecules and ions a 100 ps simulation with 2 fs time step took approximately 25 hours.

Ion-water pair correlation functions.

The ion - water pair correlation functions for all the ions were calculated in the manner described in the first paper (1). Figure 1 shows the result for all the ions studied in this paper, the distribution including only water molecules in a cone with

half angle 60° pointing into the bulk with axis parallel to the z axis. For chloride, bromide, and iodide the second peak appeared identical. The third peak in the figure contained a narrow minimum at 0.8 nm. This is indicated by the arrows in Figure 1. This feature was due to the seam in the water distribution due to the truncation of all interactions between 0.779 and 0.820 nm (see Eqn.3).

Cross correlation values.

The correlation between two variable v and w was tested by evaluating the cross correlation factor β,

$$\beta = \frac{< vw > - < v > < w >}{\sqrt{(< vv > - < v >^2)(< ww > - < w >^2)}} \tag{12}$$

where $< \phi >$ denote the average of ϕ . If v and w are completely uncorrelated, β vanishes and if v and w are highly correlated, the magnitude of β will be close to one. The cross correlation factor was used to explore the correlation between the ion's position and hydration number

Residence and Exchange Times

It was of interest to consider the mean residence time of a water molecule in a ion's hydration shell. The hydrations shell's inner and outer radii r_i and r_o respectively are determined by the minimums of the ion-water pair correlations function. A water molecule is consider to have entered the hydration shell when the water-ion separation r satisfies the relationship, $r_i(1+\delta) < r < r_o(1-\delta)$ for the first time. The parameter δ is a small number that filters out water molecules that only make very short time excursions into the shell. For this calculation δ is chosen to be 0.1 . A water molecule is then consider to have left the hydration shell when $r < r_i(1-\delta)$ or $r_o(1+\delta) < r$ In this case δ filter out events where a water molecule makes a short time excursion out of the shell. We consider the residence of this water molecule about

the ion to be the time between these two events. Then mean residence time T_R is approximated by averaging this time over all water molecules than both enter and leave the hydration shell during the simulation.

A related measure of the rate of change of the hydration shell, is the mean time of change of the hydration shell. This is simply the average time between events where the set of water molecules that constitute the hydration shell changes. In this paper a hydration shell is consider to have changed if it membership differs from the original for more than 1ps A stable hydration shell is considered to be created when its membership remains unchanged for more that 1ps. The mean time to change :.fT sub C is defined as the time to change of a stable hydration shell averaged over all stable shells created in the simulation.

III.RESULTS FOF LiF

Figure 2 shows the time evolution of the z coordinate (see left side vertical scale) of the lithium ion and fluoride ion for a time period lasting 1000 ps, in a cell also containing 214 water molecules. The broken lines at $|z| = 0.934$ nm at top and bottom of the figure indicate where the hard wall part of the surface potential begins i.e., where $V(z) = 0$. The configurations used in constructing this figure were 1 ps apart. In the starting configuration both ions were located near the cathode corresponding to time t and position z given by $(t, z) = (0, -0.5)$. In Figure 2 this corresponds to a point near the bottom left edge. Under the influence of the electric field the fluoride ion migrated the greatest distance, traversing most of the water layer to reach the anode corresponding to the broken line at $z = 0.934$ nm at the top of the figure. It took approximately 100 ps for the fluoride ion to traverse the film. It is not unreasonable to assume that during this time the solvent underwent considerable mixing, and that sufficient time lapsed sufficient time for the whole system to settle into the part of phase space describing equilibrium of the ions and associated waters. Notice that in the applied field the path of the z coordinate of the fluoride ion for the first 100 ps was not a monotonically increasing function of time. The initial movement was best described as a steady drift with superimposed high frequency jitter most likely due to interactions of the ion's primary solvent shell with surrounding solvent. This type of motion has been frequently seen in our studies of hydrated ions, and may well be typical of ions pushing through a H-bonded network. For times greater than 100 ps the time dependence of the z coordinate of both ions looks qualitatively the same. The range of positions for the ion was about 0.4 nm, not much more than the diameter of a water molecule ($\sigma = 0.31$ nm). The time averaged position of the fluoride ion was -0.668 nm, about one water diameter from the hard wall region ($|z| = 0.934$ nm).

Also shown in Figure 2 as a function of time for each ion are the numbers of water molecules in the first and second solvation shells. The data was sampled every 5 ps not every 1 ps as for the z coordinates. The radii of the solvation shells were chosen to be at the minima in the calculated ion-water pair correlation functions. For lithium these were at r = 0.2785 nm (first shell) and r = 0.500 nm (second shell). For fluoride these were at r = 0.3405 nm (first shell) and r = 0.5527 nm (second shell).

It can be seen that for lithium the first shell contained six waters with very infrequent excursions to five and seven. There was one event that lasted more than five picoseconds (see bottom right in Figure 2). The time averaged first hydration shell number was n = 6.01 . This is consistent with the calculation of Szasz et al (38), who reported the same value for bulk electrolyte, and the neutron scattering experiments of Newsome et al (39), and Hewish et al (40). The mean time to change T_C of the first solvation shell was between about 25 ps and 35 ps. This was in the range of all the other calculated values for the lithium ion with different anions. Table II summarizes the hydration water residence times for all the ions. In the case of lithium the residence time was about 100 ps for the first shell. This was about an order of magnitude larger than for the second shell, and approximately consistent with the mean time between changes (25 x 6 vs. 106 ps). These numbers are consistent with those reported for ions in a bulk environment in the interesting paper of Impey et al (15). Roughly the residence times on Li^+ ions in different LiX solutions were the same, with the larger values associated with greater statistical uncertainty. It was also three times greater than residence time for water in the first shell of fluoride ion. For the first shell there did not appear to be much correlation between position and hydration number for the first shell. The calculated correlation coefficient was 0.1. In the second shell the hydration number fluctuated between seven and sixteen, with a calculated average value of 11.4, displayed a strong correlation with distance from the electrode. The correlation coefficient of 0.5 supported the visual impression. The

mean time to change of the second shell was a not much larger than the sample interval and so not reliable, except to say that it was of the order of 1 ps. The picture that emerged was that the lithium ion and it's first shell be considered as a rather stiff or even as a rigid object, surrounded by a compliant second shell.

For fluoride the first shell contained seven waters with frequent excursions to six and seven, and a few to five. The average first shell hydration number was 6.8. The mean time between changes of the first shell was 3 ps. This was an order of magnitude smaller than for lithium. The residence time (see Table II) for hydration water was about 25 ps, in the 216 molecule system, and a little longer (33 ps) in the larger system. The differences are not large enough to be considered significant. There was no apparent correlation between first shell hydration number and position, and this was reflected in the calculated correlation of 0.18. In the second shell the hydration number fluctuated between ten and twenty two, with an average value of 15.4. There was a correlation with distance from the electrode about the same as in the second shell of lithium. The correlation coefficient was 0.57.

Figure 3 shows the density profiles for lithium and fluoride ions (normalized to unity) and water (normalized to 214) across the gap. Only configurations with time greater than 100 ps were used in accumulating this density profile. The figure also shows schematically a cartoon of the relative positions of the ions and water molecules in the first hydration shell closest to the surface. Clearly in the density 'peak' position both ions are hydrated. Not surprisingly the cation has a peak closer to the electrode since it is the ion with the smaller radius. The lithium peak position was at -0.709 nm and the fluoride was at 0.661 nm. The average positions were -0.668 nm (Li^+) and 0.628 nm (F^-). The difference 0.05 nm should be compared to the difference in Lennard-Jones radii which is 0.08 nm. The range of positions of both ions is very similar, a little less than 0.5 nm in each case. The hydrated ions have the density profile of a particle trapped in a well undergoing Brownian motion. For convenience

the main features of the densities for ions and water are collected into Tables III and IV.

The water density profile has interesting features. The larger peak at -0.803 nm was due to water in the first layer of the sample. When structure in the water distribution is compared with the ions it is clear that the larger size of the anion is responsible for the shallow minimum located near 0.66 nm. This conclusion was further substantiated by the increase in size of this feature with size of the anion. This will be seen clearly in later figures of density profiles. Calculations of the density profiles for water center of mass and the hydrogen atoms were also performed. The most interesting feature of these calculations was a small but distinct peak in the hydrogen distribution near the cathode at -0.992 nm. This was due to protons oriented towards the electrode.

Figure 4 shows density profiles calculated with the wider box (4.230 nm) containing twice as many molecules and ions. The hard wall was located at $z = \pm 1.868$ nm. Notice that the density profiles are narrower (smaller full width at half maximum). The reason for this was traced to smaller fluctuations in the positions of the ions because of weaker transcell interactions. The plots of z vs. t (time) did not show the same range of movement seen in Figure 2. Also the ions were more strongly adsorbed as judged by their peak positions, which were each closer to their respective electrodes. The peak positions relative to the hard wall are listed in Table III. For fluoride the distance from peak to hard wall was 0.13nm compared to 0.27 nm for the thinner film with 216 molecules and ions. The cartoon for the fluoride ion shows in to be closer to the electrode in Figure 4 compared to Figure 3. There was also a small shift to the electrode for the cation, but it was smaller due to stronger binding of the waters of hydration. With a cut off radius of 0.82 nm the ions did not couple directly by Coulomb interactions. There was no overlap of the range of the interactions that would be possible at times in the 2.362 nm thick sample.

There is some concern that the transcell ion attraction in the thin films may be an artifact due to the truncation of the Coulomb potentials of the sort recently described by Bader and Chandler. (41). Bader and Chandler identified an artificial, truncation induced attraction between ion of like charge, however argue that for ions of unlike charge such artifacts should be reduced. This and the fact that the transcell attraction is decreasing with film thickness argue that we are not seeing such truncation induce effects.

Figure 4 also showed that the water at the interface was quieter, as measured by the peaks and troughs in the water density profile. Major feature positions are recorded in Table IV. Note first that the density in the middle of the films was about the same. The peaks corresponding to surface water were higher at both surfaces relative to bulk for the 432 molecule system compared to the 216 system. Corroborating this notion was the deeper water exclusion trough near the fluoride ion, implying a higher degree of time averaged organization around the anion.

V. RESULTS FOR LiCl

Figure 5 shows the time evolution of the z coordinate for the lithium ion and chloride ion in a 216 molecule and ion simulation. Shown also is the time dependence of the number of water molecules in the first and second solvation shells for chloride. Lithium is not shown because it was essentially identical to the result already plotted in Figure 2. The starting configuration was the same as previously described for LiF. Note first that the time dependence of the lithium ion was qualitatively the same as in the LiF simulation and is not discussed further here. The time dependence of the z coordinate for chloride was different to fluoride. During the first 100 ps of the LiCl simulation hydrated Cl^- moved faster under the influence of the electric field and arrived at the anode sooner than fluoride did under similar conditions. This observation is significant since it is in qualitative agreement with experimentally measured transport numbers in dilute solutions (42-44). This difference was due to the larger effective radius of hydrated fluoride which binds its solvation shells more tightly than the chloride ion. In passing we note that the chloride ion z coordinate also showed jitter similar to that already described for fluoride in Figure 2.

For times greater than 100 ps the time dependence of the z coordinate of chloride looks qualitatively different from the strongly hydrated ions fluoride and lithium. First note that the chloride nucleus occasionally touches and penetrates the hard wall, which in zero electric field occurs at $|z| = 0.934$ nm. This means that chloride spends some time contact adsorbed, in contrast to fluoride which never made direct physical contact with the electrode.

Inside the box in Figure 5 the data for the first and second solvation shells of chloride was sampled every 5 ps not every 1 ps as for the z coordinates. The radii of the solvation shells were chosen to be at the minima in the calculated chloride ion-water pair correlation functions. For chloride these were at $r = 0.3758$ nm (first shell) and $r = 0.6558$ nm (second shell).

For chloride the first shell fluctuated mostly in the range five to seven with excursions to three and occasionally as high as ten (not shown in the time spanned in figure 5). The average hydration numbers for the first and second hydration shells averaged over 900 ps were 6.1 and 20.8 respectively. The first number is consistent with the pioneering studies of Dietz et al (45), who calculated 6.5 ±0.5 for the chloride ion in bulk electrolyte. There was an apparent correlation between first shell hydration number and position when the ion was close to the electrode. The calculated correlation was 0.51. For times greater than 100 ps the second shell hydration number fluctuated between twelve and thirty seven. The averaged hydration number was 20.8 for the second shell. Again there was apparent correlation with distance from the electrode and the calculated correlation was 0.81, higher than for the shells of smaller ions. The residence time for water on chloride was about 15 ps for the large system and a little smaller for the small system (see Table II). It was not dependent on shell indicating that the shells are mixing in comparable fashion consistent with water being weakly bound. This was the common description for all except the two smallest ions.

Figure 6 shows the z dependent density profiles for lithium and chloride ions (normalized to unity) and water (normalized to 214) across the film. Only configurations with times greater than 100 ps were used in accumulating these density profiles. The total simulation time was actually 1100 ps more than shown in the figure, so that for chloride statistics were collected for a total duration of 1000 ps. The main peak (average) of lithium ion occurred at -0.732 nm (-0.679 nm) with closest approach at -0.827 nm and furthest position at z = -0.283 nm. Values are tabulated in Table III. The lithium distribution resembles that for LiF quite closely.

For chloride the main peak (average) was at 0.709 nm (0.747 nm), closest at 0.968 nm and farthest point at z = 0.449 nm. The range of displacements of the chloride ion was about 0.5 nm. This was greater than shown in Figure 4 which only showed the first nanosecond, a large excursion away from the electrode occurred between 1000

ps and 1100 ps. Clearly the statistics were not sufficient to give a smooth distribution, and it is possible that the density is bimodal for a gap of 2.362 nm. If the density profile is bimodal then a calculation of the potential of mean force (46) will show two minima. This latter conclusion was also suggested by the rapidity of the transition from contact to non-contact adsorbed configuration (see Figure 4). It was considered not worthwhile to pursue this aspect further with the model used in this paper. The figure also shows schematically a cartoon of the relative positions of the ions and water molecules in the first hydration shell closest to the surface. Only when the chloride ion is furthest from the electrode at $z = 0.5$ nm, is it possible for the ion to be surrounded by a complete first solvation shell. The position of closest approach is slightly greater than 0.934 nm because the attractive electric field acts to pull the ion into the repulsive region. Also shown in Figure 6 is the water density distribution. Chloride being a larger anion than fluoride gives rise to a deeper minimum located near 0.66 nm the position of the main peak (at $z = 0.71$ nm) in the ion density. Other features in common with the fluoride simulations were the sharpness of the surface water peaks (at $|z| = 0.898$ nm) and a separate peak in the calculated proton distribution at $z = -0.992$ nm near the anode (not shown in Figure 6).

Figure 7 displays the density profile results for the thicker 4.230 nm film. Note the dramatic change in distributions for both ions. Each was found to be sharper and occupying a narrower range of Δz. The full widths at half maximum were comparable to those found for all the other thicker systems. The cartoon of hydration around the chloride ligand in Figure 7 showed that the anion was more strongly adsorbed than in the 2.3 nm film. The half widths and position shifts are consistent with the view that transcell coupling mediated by water polarization is responsible for the much broader distributions seen in the 2.36 nm films. The chloride distribution remained wider than any other ion in similar cells, suggestive of the behavior seen in the thinner film. Chloride behaved intermediate between adsorbed as a hydrated ion and adsorbed

in contact. The water exclusion zone near $z = 1.6$ nm resembled that seen already for the fluoride ion in Figure 4. All the water density profiles were remarkably similar, a fact reflected in part by the similarity in the values in Table IV.

VI.RESULTS FOR LiBr

Figure 8 displays the time dependence of the z coordinate of the lithium ion and a bromide ion during a simulation lasting 1000 ps. Unlike all the simulations presented so far this one started with an equilibrated system in which the ions were adsorbed on the electrodes. It was found that starting with the cubic lattice lead to the formation of an ion pair. The procedure used for bromide was to start with the 6 × 6 × 6 cubic array as before but in an electric field ten times stronger. The simulation was run in high field for 10 or 20 ps until both ions were in contact with the oppositely charged wall. In fields of 1.5×10^8 V/cm and greater even the cation was contact adsorbed. With the ions separated the field was then reset at 2×10^7 V/cm. Dashed horizontal lines define the hard wall region of the wall potential starting at $|z| = 0.934$ nm. This is effectively the boundary surface of the electrode. Note that the bromide ion frequently touched the boundary, and so in this model is a moderate contact adsorber, more strongly bound than chloride in Figure 4, but not as strongly bound as iodide (vide ultra).

The time dependence of the z coordinate of the lithium ion was a little different to that found for LiCl and LiBr. The range of displacements is clearly smaller, which results in the distribution being narrower. We return to this subject later.

Shown in Figure 8 as a function of time for each ion are the numbers of water molecules in the first and second solvation shells of the bromide ion. The data was sampled every 5 ps not every 1 ps as for the z coordinates. The radii of the solvation shells were chosen to be at the minima in the calculated ion-water pair correlation functions. For bromide these were at r = 0.4024 nm (first shell) and r = 0.6588 nm (second shell), same as for chloride.

For bromide the contents of the first shell fluctuated between five and six waters with infrequent excursions to four and occasional jumps to values as high as nine. The

average value was 5.6 for the first shell. The higher values were only weakly correlated with positions further from the electrode. The correlation coefficient for the first shell was calculated to be 0.37. In the second shell the hydration number fluctuated between ten and twenty six. The hydration average value was 16.8 and the correlation coefficient was 0.86, implying a strong correlation with distance from the electrode. Table II shows the residence times follow the pattern established for chloride.

Figure 9 shows the distribution of Li^+, Br^-, and 214 water molecules in a strong electric field ($2x10^7$ V/cm) across the gap between the charged plates. The wall potential is shown for reference. Circles have the Lennard-Jones radii for the ions and water. The configurations were collected in the time interval 100 ps < time < 1000 ps. The range of bromide positions was: farthest z = 0.661 nm, closest z = 0.968 nm, and peak (average) position at approximately 0.874 nm (-0.861 nm). At the closest approach the negative ion lay inside the repulsive regime of the wall potential. In this simulation the anion engages in moderate contact adsorption, stronger than chloride but not as strong as in the case of iodide. Note the again the presence of the shallow minimum in the water distribution near the average position of the anion. This minimum is slightly more pronounced than in the case of chloride. It is due to exclusion of water molecules from the interface by the larger volume of the ion.

The results of simulations with a twelve (4.230 nm) water layer system are shown in Figure 10. The trend to contact adsorption with larger ionic size was continued. Again there was a narrow lithium distribution characteristic of the thicker film. What was of interest in comparing the density profiles in Figures 9 and 10, was their similarity. In all the other LiX systems the 2.36 and 4.23 nm films show how the transcell interaction drops in going to the thicker cell.

The transcell interactions between Li^+ and Br^- appeared weaker in thin cell compared say to LiF and LiCl. As with LiI, to be discussed in the next section, it appeared that as contact adsorption increased then the more the anion decoupled from the bulk

water and the smaller the perturbation on the cation due to movement of the anion perpendicular to the surface. As seen from the Figure 10 and the positions tabulated in Table III the lithium cation peak at z = -1.692 nm had moved a little closer to the hard wall, and the density profile was somewhat sharper. Indeed the lithium position was close to that for a lithium ion without an anion but trapped against the cathode by the static field used in all these simulations (6).

VII. RESULTS FOR LiI

The case of lithium iodide solutions at constant energy were described in the first (1) paper. New results are presented here for simulations done at constant temperature. Iodide represents the extreme case of contact adsorption. Experimentally iodide is known to contact adsorb on metals at potentials corresponding to thermodynamically stable electric double layers. in contrast to lithium ions which do not. Time dependence of the z coordinate of the lithium ion and a iodide ion during a simulation lasting 400 ps is shown in Figure 11. The sampling interval in these calculations was 0.5 ps, smaller than in all the previous calculations described so far which were all at 1.0 ps. The starting configuration was one previously obtained in the earlier study (1). As before the dashed horizontal lines define the repulsive region of the wall potential starting at $|z| = 0.934$ nm. This is effectively the boundary surface of the electrode. Note that the iodide ion spends almost all its time at the boundary, and in this model is classified as a strong contact adsorber. It makes only short time excursions away from the surface, and is rarely found more than 0.1 nm removed from contact.

Also shown in Figure 11 as a function of time for the iodide ion are the numbers of water molecules in the first and second solvation shells. The data was sampled every 2.5 ps not every 5 ps as for the hydration number plots in the figures for LiF, LiCl, and LiBr. The radii of the solvation shells taken from the calculated ion-water pair correlation functions were at $r = 0.4289$ nm (first shell) and $r = 0.6765$ nm (second shell).

For iodide the first shell fluctuated between two and eight, with four, five and six being the most frequent occupation number. The average value was 5.4 for the first shell with a correlation of 0.29 (weak, corresponding to no apparent correlation visible in Figure 11) between first shell hydration number and position. Because the ion was so strongly adsorbed the correlation was small. In the second shell the hydration

number fluctuated between eleven and twenty five. The average value was 16.8. A weak correlation with distance from the electrode was apparent, the calculated correlation was 0.63.

As shown in Figure 12 the essential features of the iodide distribution emerge even after a simulation running for 400 ps. The distribution of the Li^+ ion and the 214 water molecules looks very similar to LiF and LiCl solutions. In this simulation the anion exhibits strong contact adsorption. The anion density profile was sharply peaked (average) at z = 0.921 nm (0.886 nm) very close to the hard wall. The point of closest approach was 0.992 nm, and that farthest from the electrode was at 0.685 nm. The water distribution in Figure 9 has more noise than the one shown in Figure 6 for LiCl solution because of poorer statistics resulting from a simulation time of 400 ps duration. In spite of this the shallow minimum in the water distribution due to the ion displacing water was clearly visible near 0.70 nm. Table IV gives the salient features of all the water distributions.

In Figure 13 the results of the thick film density profile are displayed. As before the system was allowed to equilibrate for 100 ps before averaging over configurations collected during the next 900 ps. The iodide density distribution was the sharpest, of all the halide profiles for all the systems studied here. The peak value of nearly 14 nm^{-1} in the thick film compared to 11 nm^{-1} in the six layer film. A comparison of water density profiles showed them all to be very similar, with all the distribution differences occurring near the walls. The differences that did exist seemed to be related to the degree and strength of hydration of the adsorbed ions. Consistent with weaker coupling across this thicker film, the water distribution near the cathode where the Li^+ was adsorbed were superimposable for different anions in systems with 432 molecules and ions.

VIII. RESULTS FOR WEAKER FIELDS

This section resumes the discussion of the quality of water and ion parameters for surface studies begun in the introduction.

It has been pointed out (8) that small ion parameters over estimate the of hydration by as much as 25%. Consequently in the field we are using $2x10^7$ V/cm in our simulations, the ability of small ions like fluoride F^- and lithium Li^+ to adsorb with intact primary solvation shell is exaggerated compared to the larger ions. The magnitude of this field is at the upper end for stable electrochemical double layers so it is of interest to know what happens in weaker fields.

However it is an experimental fact that small ions like Li^+ and fluoride F^- do not chemisorb on to metals in the double region of electrode potentials, and this phenomenon is attributed to their strongly held primary solvation shells. There are even anions (PF_6^-, BF_6^- and ClO_4^-) that adsorb more weakly than fluoride (5), in that they distrurb the interface even less (lower capacitance). Consequently although the ST2 parameters for Li^+ do not qualitatively model the adsorption process at the value of the static field used here, the series of Heinzinger's anion parameters does model adsoption changes along the series. We do not expect this modelling to be quantitative, for example by predicting the value of the threshold field above which the lithium ion to be contact adsorbed.

To explore the static field dependence we calculated the density profile for a single Li^+ ion with 215 water molecules and a single I^- ion in 215 ST2 waters, for different values of the applied field. All other conditions in these simulations were the same as before.

For fields about seven times higher (ca.$1.5x10^8$V/cm), like the ones used in the calculations of Brodsky and Reinhardt (30, 31), the lithium ion was contact adsorbed and it was observed that all the waters of the film oriented with dipoles ||z. The

behaviour in the regime of weaker fields is more relevant to the present study. As the field was weakened the density profile of Li^+ ion shifted towards the middle of the water film. In zero field the density profile $\rho_{ion}(z)$ was a broad bell-like distribution with the tails reaching out to about $|z| = 0.5$nm. This result is consistent with that reported by Wilson et al (47) for a single sodium ion in a 2.0 nm thick film of water with two liquid - vapour boundaries, and can be interpreted as the ions migrating to maximize their polarization energy in the solvent. Relaxation times were found to be longer than 1 ns, because of the large configuration space explored. Consequently it was not possible to get good statistics by accumulating configurations with brute force dynamics. This problem could be better tackled using umbrella sampling (24) or some scheme to simplify the long time dynamics like those used to studied polypeptides (48).

In the case of iodide the peak in the density profile $\rho_{ion}(z)$ for a given field always occurred at a point closer to the charged wall than was the case for lithium ion. This is consistent with the previous calculations for I^- ion, and suggests that the establishment of the solvent structure around this large anion occurs gradually as the field is weakened and the ion pulls pulls back from the wall.

What can be concluded from these results? First because of differences in ionic radii the smaller ions will be more strongly hydrated than larger ions. As the strength of the field is increased ions with more strongly bound solvation shells will tend to spend more time contact adsorbed. Conversely, in the absence of a strong universally binding interaction such as an image interaction, the adsorbed ions will shift away from the electrode as the field is weakened. An exception will occur for large hydrophobic ions which might remain adsorbed in a configuration that maximized solvent entropy (it is well established that large neutral organics eg., benzene, are adsorbed most strongly at the potential of zero charge) (49).

IX. SUMMARY

The simulations described here have revealed some of the static and dynamical complexities of the adsorption of hydrated ions onto charged surfaces. The main features were as follows. i) The small ions Li^+ and F^- did not make contact with electrode in fields of $2x10^7$V/cm because of their strongly bound first solvation shells. There was a balance between electric and Lennard-Jones attraction and thermal fluctuations. In the thin film polarization coupling mediated by water molecules increased the size of the fluctuations experienced by the ions. ii) In the model used here chloride was the first ion to exhibit contact adsorption. In the 2 nm film it appeared to have a bimodal distribution. iii) The presence of adsorbed ions implies the presence of localized water held in place by the field of the ion and it's associated hydrogen bond network. The presence of large interfacial ions also means there is a depletion zone where fewer waters are located. iv) The time dependence of the first shell hydration numbers for lithium and fluoride corroborate the picture. The residence time of a water molecule on lithium ion was a factor of four longer compared to fluoride. The first solvation shell of chloride and the bigger ions were found to be all very dynamic with residence times around 10 ps according to the model used here. Exchange of water between the first shell and the bulk was less than about 1ps.

Finally we point out that their are significant physical effects not modeled in the present study. In particular rigid non polarizable models exhibit dielectric saturation. To more accurately account for relaxation around small ion core one clearly needs to enhance the models in significant ways outside the scope of the present study. In the extremely high fields near small ion cores water molecules will distort electronically and geometrically. To account for these effects commonly adopted enhancements include replacement of the repulsive r^{-12} core potentials with softer ones fashioned after exp(-ar), or better still a sum of exponentials obtained from a quantum chemistry

calculation, polarizable ions and neutral water molecules, and flexible water molecules. Work on incorporating these effects in useable models is in progress in our laboratory.

ACKNOWLEDGEMENT

This research was supported in part by the Office of Naval Research. R.Rafey is thanked for assistance with visualization graphics.

References

(1) J. N. Glosli and M. R. Philpott, J. Chem. Phys. **96**, 6962-6969 (1992).

(2) J. O. Bockris and A. K. Reddy, *Modern Electrochemistry, Vol.2* (Plenum Press, New York, 1973).

(3) R. Parsons, Chem. Rev. **90**, 813-826 (1990).

(4) C. Gutierrez and C. Melendres, *Spectroscopic and Diffraction Techniques in Interfacial Electrochemistry, NATO ASI Series C* (Kluwer,Dordrecht,Holland, 1990).

(5) G. Valette, J. Electroanal. Chem. **122**, 285 - 297 (1981).

(6) J. N. Glosli and M. R. Philpott, unpublished calculations (1992).

(7) F. H. Stillinger and A. Rahman, J. Chem. Phys. **60**, 1545 (1974).

(8) W. L. Jorgensen, J. Chandrasekhar, J. D. Madura, R. W. Impey, and M. L. Klein, J. Chem. Phys. **79**, 926-935 (1983).

(9) H. J. Berendsen, J. R. Grigera, and T. P. Straatsma, J. Phys. Chem. **6269**, 6267 (1987).

(10) J. A. Barker, C. T. Rettner, and D. S. Bethune, Chem. Phys. Lett. **188**, 471 - 476 (1992).

(11) J. L. Stickney, S. D. Rosasco, G. N. Salaita, and A. T. Hubbard, Langmuir. **1**, 66 - 71 (1985).

(12) M. F. Toney, J. G. Gordon, and O. R. Melroy, SPIE Proceedings **1550**, xxx - xxx (1991).

(13) T. Tadjeddine, D. Guay, M. Ladouceur, and G. Tourillon, Phys. Rev. Lett. **66**, 2235 - 2238 (1991).

(14) M. Mezei and D. L. Beveridge, J. Chem. Phys. **74**, 6902 - 6910 (1981).

(15) R. W. Impey, P. A. Madden, and I. R. McDonald, J. Phys. Chem. **87**, 5071 - 5083 (1983).

(16) J. Chandrasekhar, D. C. Spellmeyer, and W. L. Jorgensen, J. Amer. Chem. Soc. **106**, 903-910 (1983).

(17) J. O. Brockris, M. A. Devanathan, and K. Müller, Proc. Roy. Soc.(London) **A274**, 55-79 (1963.).

(18) R. F. Lane and A. T. Hubbard, J. Phys. Chem. **79**, 808 - 815 (1975).

(19) A. T. Hubbard, Chem. Rev. **88**, 633 - 656 (1988).

(20) M. R. Deakin and O. Melroy, J. Electroanal. Chem. **239**, 321 - 331 (1988).

(21) M. R. Deakin and O. Melroy, J. Electroanal. Chem. **243**, 343 - 351 (1988).

(22) G. I. Szasz, K. Heinzinger, and W. O. Riede, Z. Naturforsch. **36a**, 1067 - 1075 (1981).

(23) E. Spohr and K. Heinzinger, J. Chem. Phys. **84**, 2304-2309 (1986).

(24) D. A. Rose and I. Benjamin, J. Chem. Phys. **95**, 6856-6865 (1991).

(25) H. J. Berendsen, J. P. Postsma, W. F. van Gunsteren, and J. Hermans, *Intermolecular Forces* (Reidel, Dordrecht, Holland, 1981), p. 331.

(26) E. Spohr and K. Heinzinger, Ber. Bunsenges. Phys. Chem. **92**, 1358-1363 (1988).

(27) K. Heinzinger, *Computer Modelling of Fluids Polymers and Solids*, (Kluwer,Dordrecht, 1990), pp. 357-404.

(28) J. Seitz-Beywl, M. Poxleitner, and K. Heinzinger, Z. Naturforsch. **46A**, 876 (1991).

(29) P. Bopp, G. Jansco, and K. Heinzinger, Chem. Phys. Letters **98**, 129-133 (1983).

(30) M. Watanabe, A. M. Brodsky, and W. P. Reinhardt, J. Phys. Chem. **95**, 4593 (1991).

(31) A. M. Brodsky, M. Watanabe, and W. P. Reinhardt, Electrochimica Acta **36**, 1695-1697 (1991).

(32) S. Zhu and G. W. Robinson, J. Chem. Phys **94**, 1403-1410 (1991).

(33) S. Zhu, T. G. Fillingim, and G. W. Robinson, J. Phys. Chem. **95**, 1002-1006 (1991).

(34) J. Hautman, J. W. Halley, and Y. Rhee, J. Chem. Phys. **91**, 467-472 (1989).

(35) O. Steinhauser, Mol. Phys. **45**, 335-348 (1982).

(36) C. Y. Lee, J. A. McCammon, and P. J. Rossky, J. Chem. Phys. **80**, 4448-4455 (1984).

(37) M. P. Allen and D. J. Tildesley, *Computer Simulation of Liquids* (Oxford University Press, Oxford, 1989), pp. 88-90.

(38) G. I. Szasz, K. Heinzinger, and G. Palinkas, Chem. Phys. Lett. **78**, 194 (1981).

(39) J. R. Newsome, J. E. Enderby, and G. W. Neilson, J. Phys. C **13**, L923 (1980).

(40) N. A. Hewish, J. E. Enderby, and W. S. Howells, J. Phys. C 16, 1777 (1983)

(41) J. S. Bader and D. Chandler, J. Phys. Chem. **96**, 6423 - 6427 (1992).

(42) J. Burgess, *Metal Ions in Solution* (Halsted Press, John Wiley, New York, 1978).

(43) A. L. Horvath, *Handbook of Aqueous Electrolyte Solution* (Halsted Press, John Wiley, New York, 1985), pp. 196, 240.

(44) J. O. Bockris and A. K. Reddy, *Modern Electrochemistry, Vol.1* (Plenum Press, New York, 1973).

(45) W. W.Dietz, W. W.O.Reide, and K. K.Heinzinger, Z. Naturforsh. **37A**, 1038 (1982).

(46) G. Ciccoti, M. Ferrario, J. T. Hynes, and R. Kapral, Chem. Phys. **129**, 241-251 (1989).

(47) M. A. Wilson, A. Pohorille, and L. R. Prattd, Chem. Phys. **129**, 209 - 212 (1989).

(48) G. R. Hu, G. R. Flemming, K. F. Freed, and A. Perico, Chem. Phys. **158**, 395 - 408 (1991).

(49) F. Anson, Accts Chem. Res. **8**, 400-407 (1975).

Table I The interaction parameters ($q, \varepsilon, \sigma, A, B$) and mass ($m$) for all atoms used in the simulations, where $q_o = e$, $\varepsilon_o = 1 KJ/mole$, $\sigma_o = 1 nm$, $A_o = 17.447 \times 10^{6} KJ \cdot nm^6/mole$, $B_o = 76.144 \times 10^{3} KJ \cdot nm^3/mole$, and $m_o = 1 AMU$. The ε and σ for unlike atom pairs is formed from the combination rules, $\varepsilon_{AB} = \sqrt{(\varepsilon_{AA}\varepsilon_{BB})}$ and $\sigma_{AB} = (\sigma_{AA} + \sigma_{BB})/2$.

	q/q_o	$\varepsilon/\varepsilon_o$	σ/σ_o	m/m_o	A/A_o	B/B_o
O_ST2	0.0000	0.316	0.310	16.0	1	1
H_ST2	0.2357	0.000	0.000	1.000	0	0
PC_ST2	− 0.2357	0.000	0.0	0.0	0	0
Li	1.0000	0.149	0.237	6.9	1	1
F	− 1.0000	0.050	0.400	19.0	1	1
Cl	− 1.0000	0.168	0.486	35.5	1	1
Br	− 1.0000	0.270	0.504	79.9	1	1
I	− 1.0000	0.408	0.540	129.9	1	1

Table II. Summary of hydration water residence times with the one sigma errors for LiX (X = F,Cl,Br,I) in water films with 216 molecules (2.362nm) and 432 molecules (4.320nm).

	LiF	LiCl	LiBr	LiI
2.362 nm film with 216 molecules				
Li^+ ion, 1st shell	122±25	168±43	115±43	
Li^+ ion, 2nd shell	12±0.5	12±0.4	12±0.5	
X^- ion, 1st shell	25±1.8	12±0.6	11±0.6	
X^- ion, 2nd shell	13±0.4	13±0.4	12±0.4	
4.320 nm film with 432 molecules				
Li^+ ion, 1st shell	106±14	97±12	87±17	130±22
Li^+ ion, 2nd shell	10±0.3	9±0.3	10±0.3	9±0.3
X^- ion, 1st shell	33±2.7	16±1.2	14±0.8	11±0.6
X^- ion, 2nd shell	15±0.6	16±0.6	16±0.6	15±0.5

Table III. Summary of density profile results of halide ions in two water films. All positions relative to closest wall at |z| = 0.934 (for 2.362nm film) and |z| = 1.868nm (for 4.320nm film)

	Li^{+} [a]	F^{-}	Cl^{-}	Br^{-}	I^{-}
2.362nm film					
$z_{near} - z_h$ [b]	+0.084	-0.084	+0.034	+0.058	+0.058
$z_{pk} - z_h$ [c]	+0.225	-0.273	-0.225	-0.036	-0.013
$z_{far} - z_h$ [d]	+0.580	-0.556	-0.509	-0.320	-0.249
4.320nm film					
$z_{near} - z_h$ [b]	+0.044	-0.007	+0.062	+0.062	+0.062
$z_{pk} - z_h$ [c]	+0.202	-0.176	-0.044	-0.017	-0.017
$z_{far} - z_h$ [d]	+0.414	-0.440	-0.335	-0.308	-0.202

a lithium from LiF simulation

b z_{near}, point of nearest approach to electrode

c z_{pk}, position of peak in the density

d z_{far}, position of farthest point from electrode

Table IV. Summary of water density profile results for LiX (X = F,Cl,Br,I) two water films. All positions measured in nm relative to nearest hard wall at $|z_h| = 0.934nm$ (for 2.362nm film) and $|z_h| = 1.808$ (for 4.320nm film). The number in parentheses is the value in nm^{-1} of the density profile

	LiF	LiCl	LiBr	LiI
2.362nm film				
Peak on anion side	-0.060 (147)	-0.036 (143)	-0.036 (142)	-0.036 (135)
Minimum on anion side	-0.273 (103)	-0.273 (95)	-0.296 (93)	-0.273 (91)
Peak on cation Side	0.036 (133)	0.036 (140)	0.036 (138)	0.036 (138)
4.320nm film				
Peak on anion side	-0.044 (157)	-0.044 (150)	-0.044 (152)	-0.044 (141)
Minimum on anion side	-0.255 (96)	-0.282 (93)	-0.255 (90)	-0.255 (87)
Peak on cation Side	0.044 (146)	0.044 (149)	0.017 (151)	0.017 (147)

FIGURE CAPTIONS

Figure 1. Ion-water pair correlation functions for lithium and the halide ions. The four correlation functions for the lithium ions are superimposed showing their essential equivalence. For chloride, bromide, and iodide the second peak near 0.55 nm are also essentially the same within numerical error. The dip at 0.82 nm indicated by the arrows was due to the truncation function.

Figure 2. Time dependence of the z coordinate of the lithium ion and a fluoride ion during a simulation lasting 1000 ps. At time t = 0 ps both ions start out near the cathode. It takes the anion about 100 ps to migrate across the gap. Note that the electric fields keep the ions separated and restricted to vicinity of their respective electrodes. The ions are not free to diffuse throughout the gap. Dashed horizontal lines define the beginning of the hard wall repulsive region of the potential starting at |z| = 0.934 nm. This is effectively the boundary surface of the electrode.

Figure 3. Distribution of Li^+, F^-, and 214 water molecules in a strong electric field ($\sim 2 \times 10^7$ V/cm) across the gap between the charged plates. Wall potential shown for reference. Circles are Lennard-Jones radii for the ions and water. In this simulation the anion never contact adsorbs. Contrast this with the results of the simulation for LiCl, LiBr, and LiI. Note the shallow minimum in the water distribution near the average position of the anion.

Figure 4. Distribution of Li^+, F^-, and 430 water molecules in a strong electric field ($\sim 2 \times 10^7$ V/cm) across the gap between the charged plates. Wall potential

shown for reference. Circles are Lennard-Jones radii for the ions and water. In this simulation the anion never contact adsorbs. Contrast this with the results of the simulation for LiCl, LiBr, and LiI. Note the shallow minimum in the water distribution near the average position of the anion.

Figure 5. Time dependence of the z coordinate of the lithium ion and a a chloride ion during a simulation lasting 1000 ps. At time t = 0 ps both ions start out near the cathode. It takes the anion less than 100 ps to migrate across the gap. Note that the electric fields keep the ions separated and restricted to vicinity of their respective electrodes. The ions are not free to diffuse throughout the gap. Dashed horizontal lines define the hard wall region of the potential starting at |z| = 0.934 nm. This is effectively the boundary surface of the electrode. Unlike fluoride the chloride ion does touch the boundary, and in this model is able to contact adsorb in weak fashion.

Figure 6. Distribution of Li^+, Cl^-, and 214 water molecules in a strong electric field ($\sim 2 \times 10^7$ V/cm) across the gap between the charged plates. Wall potential shown for reference. Circles are Lennard-Jones radii for the ions and water. In this simulation the anion makes weak contact adsorption. Contrast this with the results of the simulation for LiBr and LiI, where the contact adsorption is more frequent and therefore stronger. Note the shallow minimum in the water distribution near the average position of the anion.

Figure 7. Distribution of Li^+, Cl^-, and 430 water molecules in a strong electric field ($\sim 2 \times 10^7$ V/cm) across the gap between the charged plates. Wall potential shown for reference. Circles are Lennard-Jones radii for the ions and water. In this simulation the anion makes weak contact adsorption. Contrast this

with the results of the simulation for LiBr and LiI, where the contact adsorption is more frequent and therefore stronger. Note the shallow minimum in the water distribution near the average position of the anion.

Figure 8. Time dependence of the z coordinate of the lithium ion and a bromide ion during a simulation lasting 1000 ps. Note that the electric fields keep the ions separated and restricted to vicinity of their respective electrodes. The ions are not free to diffuse throughout the gap. Dashed horizontal lines define the repulsive region of the wall potential starting at $|z| = 0.934$ nm. This is effectively the boundary surface of the electrode. Note that the bromide ion frequently touches the boundary, and so in this model is a moderate contact adsorber.

Figure 9. Distribution of Li^+, Br^-, and 214 water molecules in a strong electric field ($\sim 2 \times 10^7$ V/cm) across the gap between the charged plates. Wall potential shown for reference. Circles are Lennard-Jones radii for the ions and water. In this simulation the anion engages in moderate contact adsorption. Contrast this with the results of the simulation for LiF where there is no contact and LiI where the iodide makes strong contact. Note the shallow minimum in the water distribution near the average position of the anion.

Figure 10. Distribution of Li^+, Br^-, and 430 water molecules in a strong electric field ($\sim 2 \times 10^7$ V/cm) across the gap between the charged plates. Wall potential shown for reference. Circles are Lennard-Jones radii for the ions and water. In this simulation the anion engages in moderate contact adsorption. Contrast this with the results of the simulation for LiF where there is no

contact and LiI where the iodide makes strong contact. Note the shallow minimum in the water distribution near the average position of the anion.

Figure 11. Time dependence of the z coordinate of the lithium ion and a iodide ion during a simulation lasting 400 ps. Note that the electric fields keep the ions separated and restricted to vicinity of their respective electrodes. The ions are not free to diffuse throughout the gap. Dashed horizontal lines define the hard wall region of the potential starting at $|z| = 0.934$ nm. This is effectively the boundary surface of the electrode. Note that the iodide ion spends almost all its time at the boundary, and in this model is classified as a strong contact adsorber. It makes only short time excursions away from the surface.

Figure 12. Distribution of Li^+, I^-, and 214 water molecules in a strong electric field ($\sim 2 \times 10^7$ V/cm) across the gap between the charged plates. Wall potential shown for reference. Circles are Lennard-Jones radii for the ions and water. In this simulation the anion exhibits strong contact adsorption. The density profile is sharply peaked very close to the repulsive wall. Contrast this with the results of the simulation for LiF where there is no contact. Note the shallow minimum in the water distribution near the average position of the anion.

Figure 13. Distribution of Li^+, I^-, and 432 water molecules in a strong electric field ($\sim 2 \times 10^7$ V/cm) across the gap between the charged plates. Simulation time 1000ps. Wall potential shown for reference. Circles are Lennard-Jones radii for the ions and water. In this simulation the anion exhibits strong contact adsorption. The density profile is sharply peaked very close to the repulsive

wall. Contrast this with the results of the simulation for LiF where there is no contact. Note the shallow minimum in the water distribution near the average position of the anion.

F1

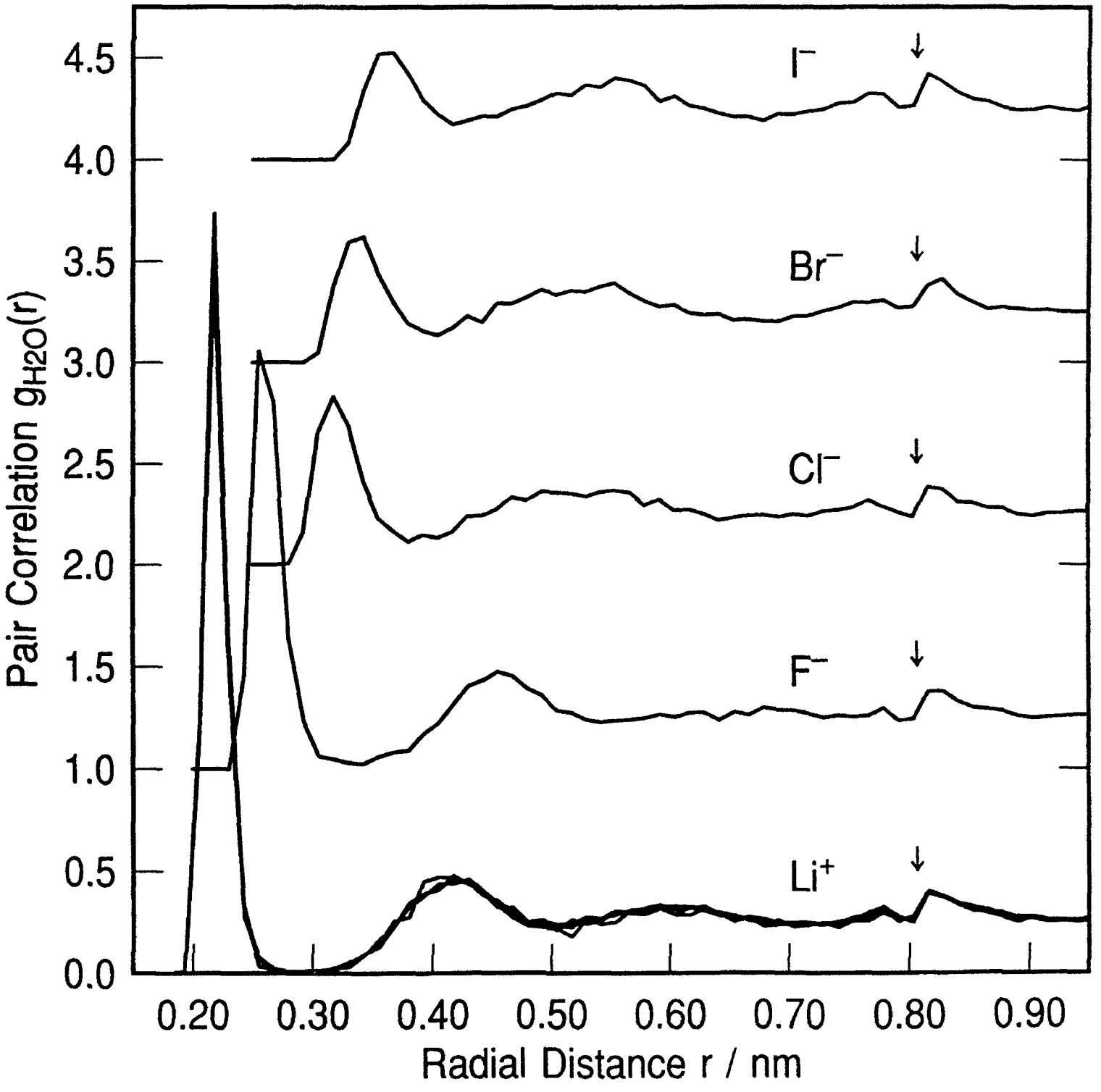
Pair Correlation $g_{H2O}(r)$
4.5
4.0
3.5
3.0
2.5
2.0
1.5
1.0
0.5
0.0
I^-
Br^-
Cl^-
F^-
Li^+
0.20
0.30
0.40
0.50
0.60
0.70
0.80
0.90
Radial Distance r / nm

F2

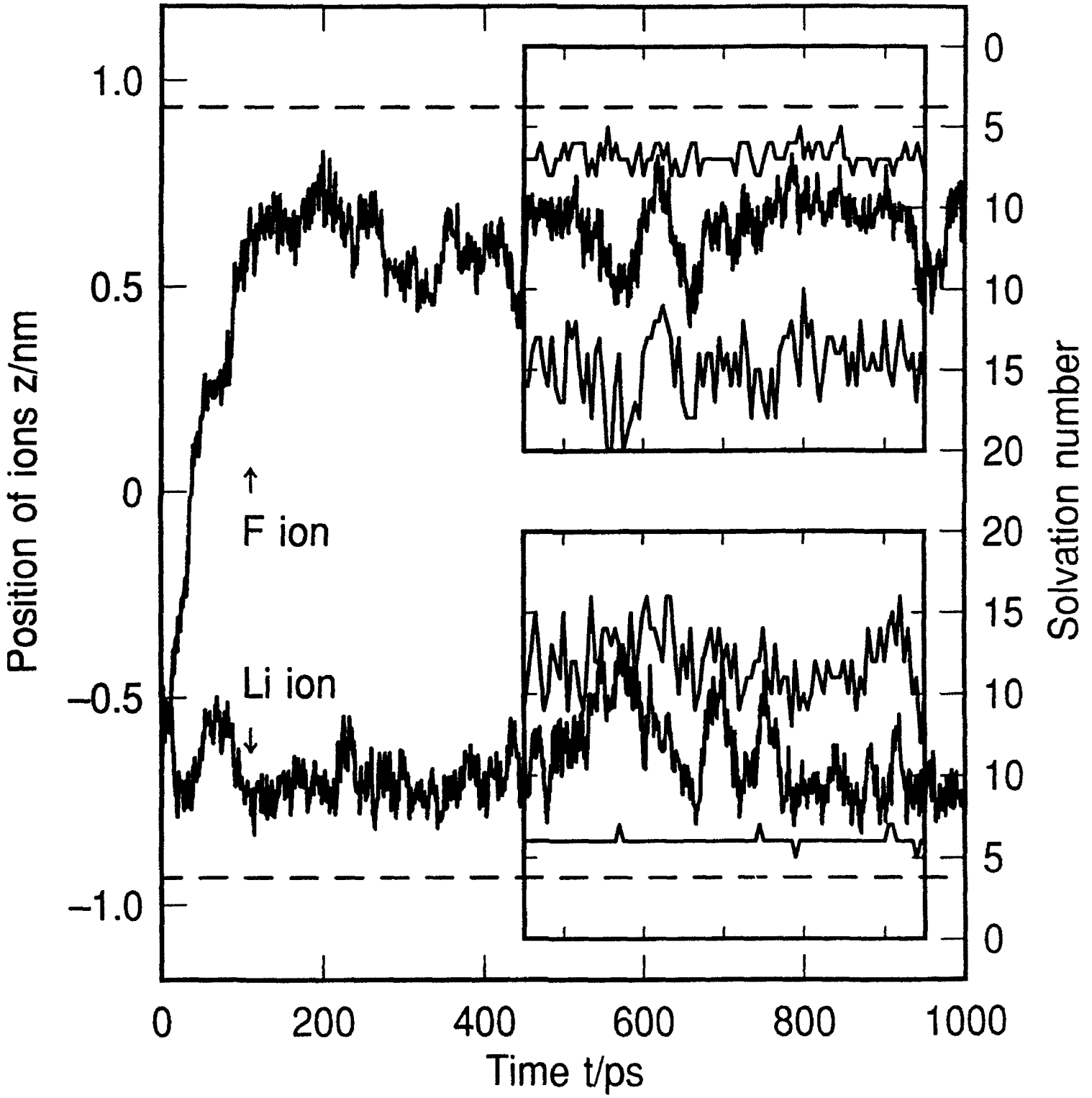
1.0
0.5
0
−0.5
−1.0
Position of ions z/nm
↑
F ion
Li ion
↓
0
5
10
10
15
20
20
15
10
10
5
0
Solvation number
0
200
400
600
800
1000
Time t/ps

F3

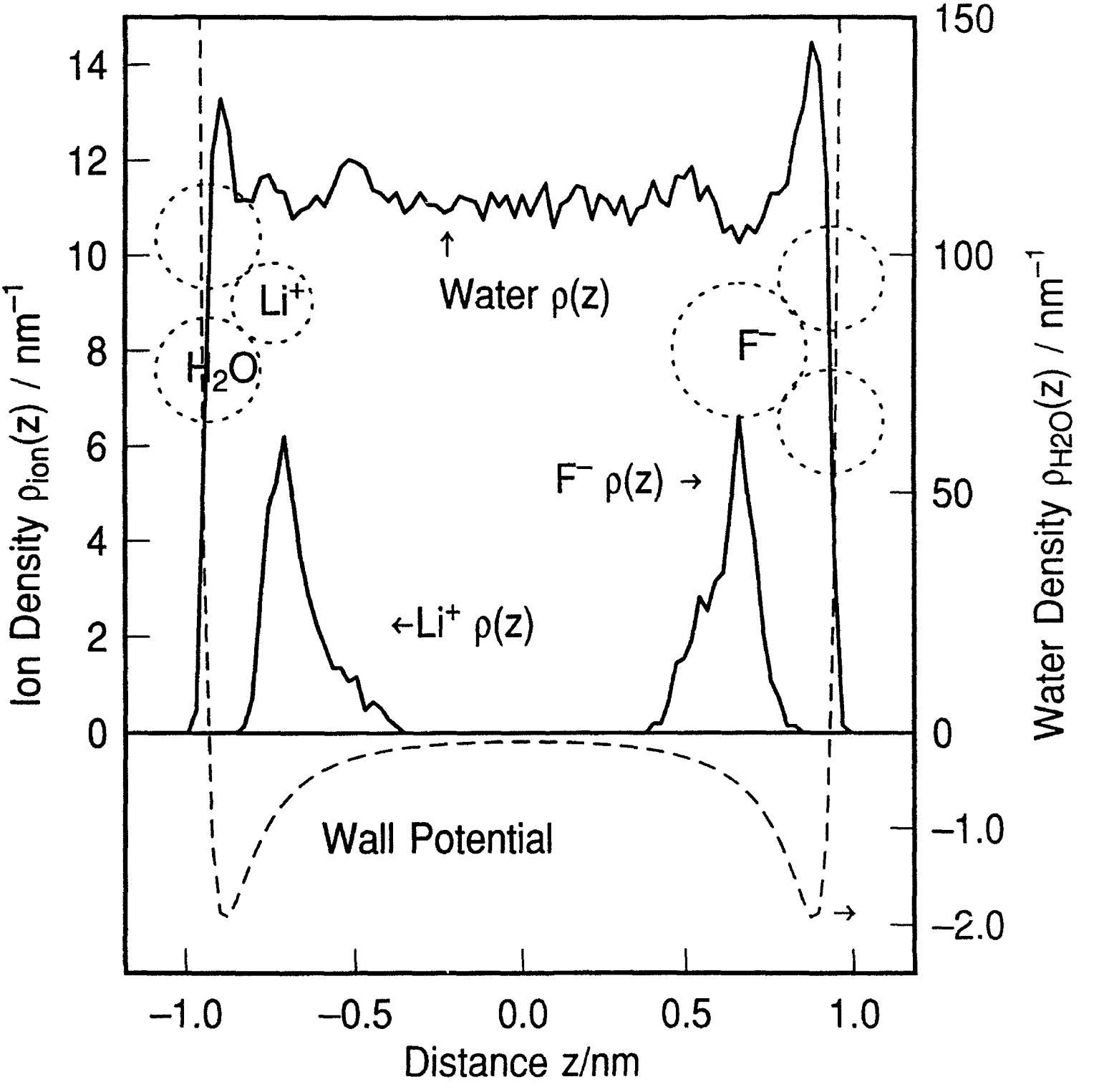
Ion Density $\rho_{ion}(z)$ / nm^{-1}
Water Density $\rho_{H2O}(z)$ / nm^{-1}
Distance z/nm
Water ρ(z)
Li+
H2O
F−
F− ρ(z) →
←Li+ ρ(z)
Wall Potential
14
12
10
8
6
4
2
0
150
100
50
0
−1.0
−2.0
−1.0
−0.5
0.0
0.5
1.0

F4

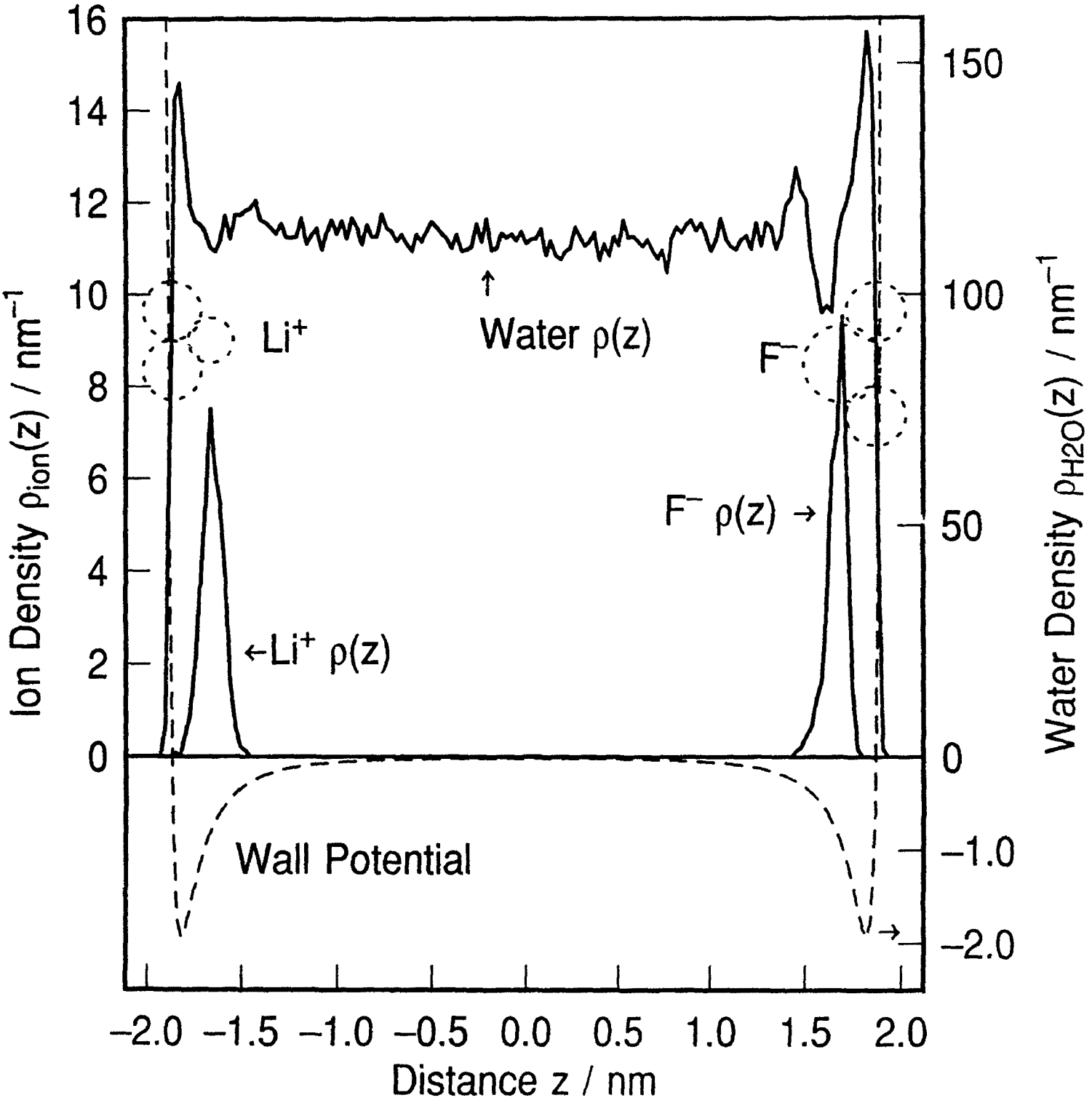
16
14
12
10
8
6
4
2
0
150
100
50
0
−1.0
−2.0
Li+
Water ρ(z)
F−
F− ρ(z) →
←Li+ ρ(z)
Wall Potential
→
−2.0 −1.5 −1.0 −0.5 0.0 0.5 1.0 1.5 2.0
Distance z / nm
Ion Density ρion(z) / nm−1
Water Density ρH2O(z) / nm−1

F5

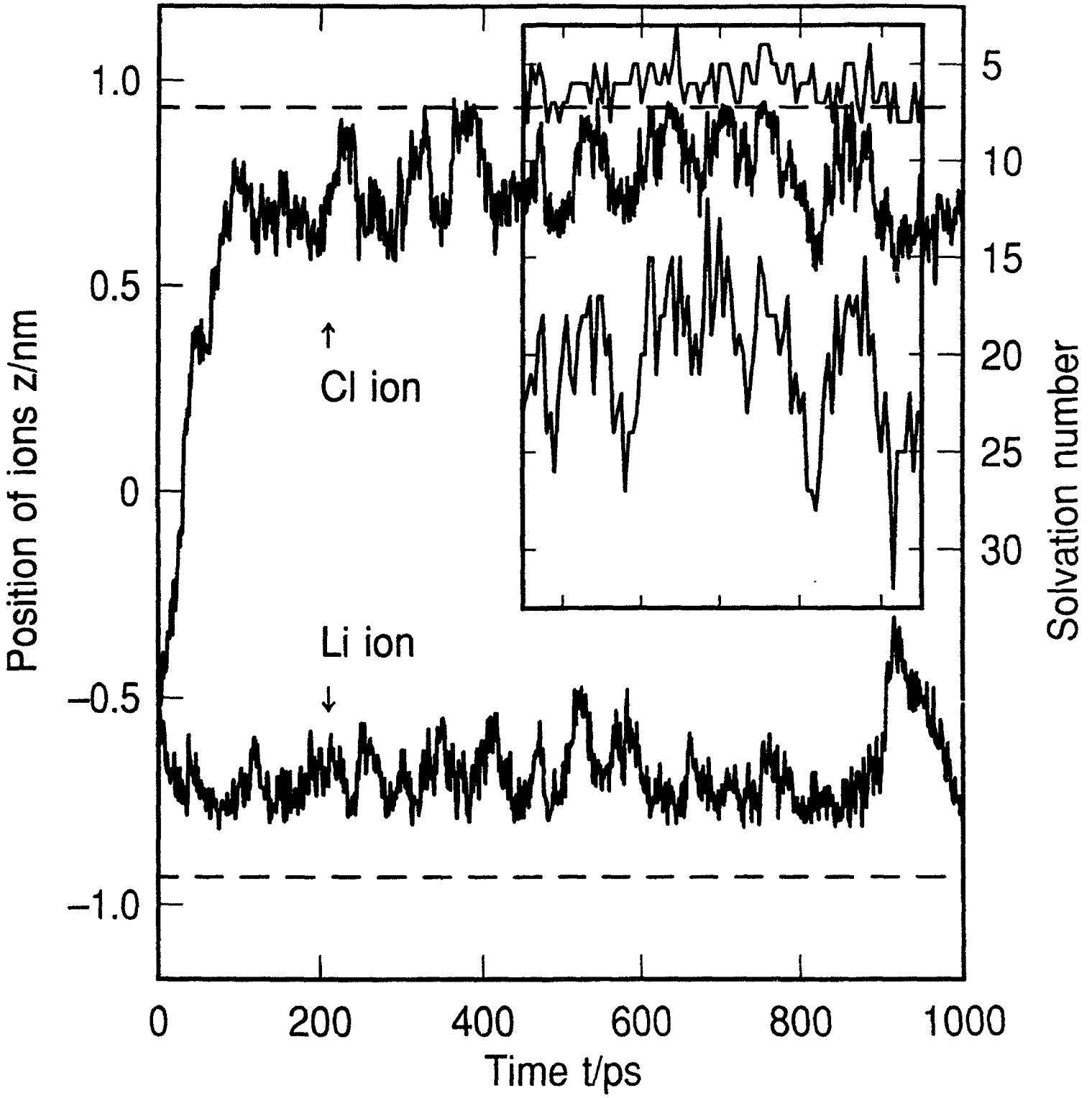
1.0
0.5
0
−0.5
−1.0
Position of ions z/nm
↑
Cl ion
Li ion
↓
5
10
15
20
25
30
Solvation number
0
200
400
600
800
1000
Time t/ps

F6

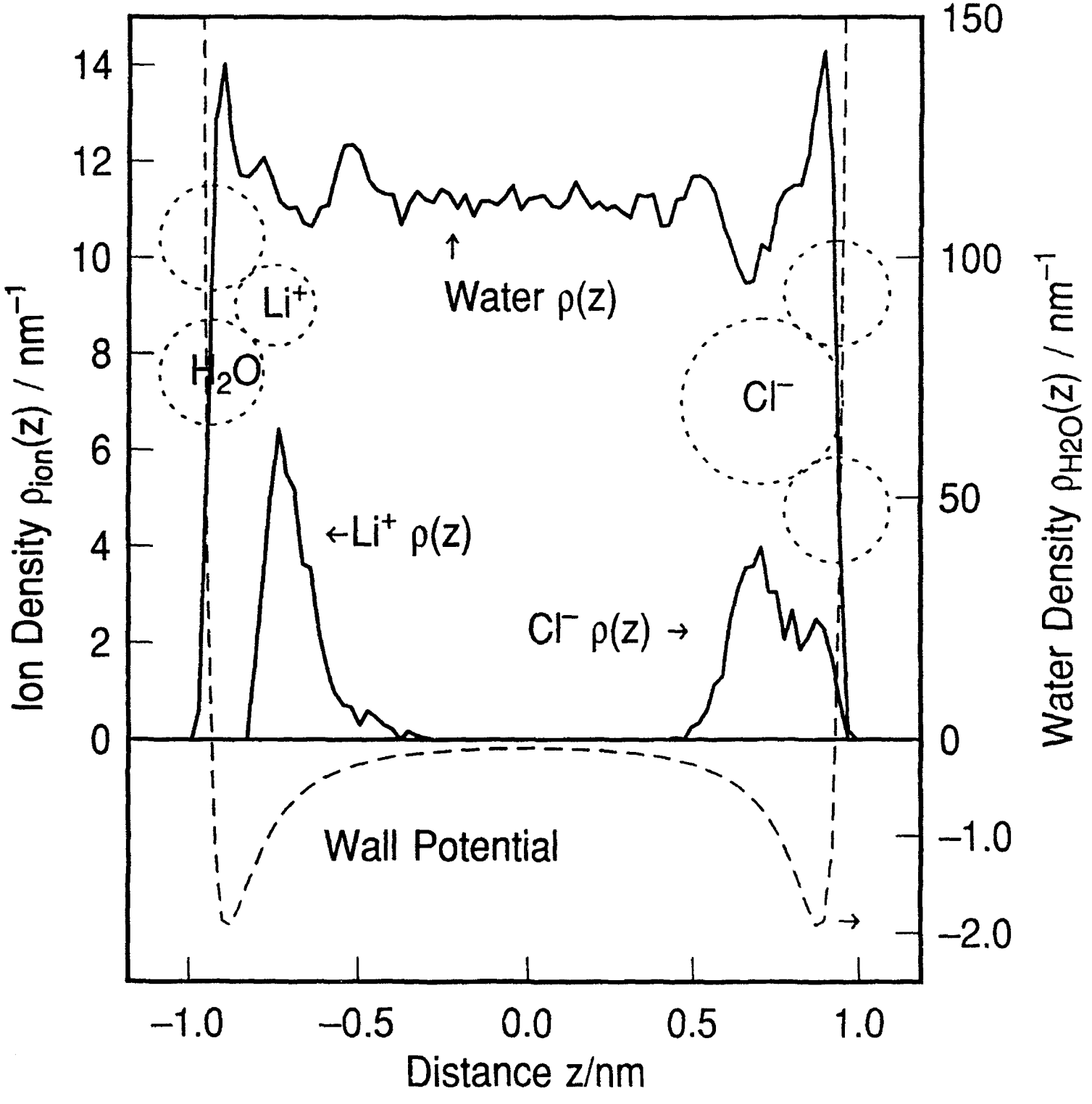
Ion Density $\rho_{ion}(z)$ / nm^{-1}
Water Density $\rho_{H2O}(z)$ / nm^{-1}
Distance z/nm
Water ρ(z)
Li+
H2O
Cl−
←Li+ ρ(z)
Cl− ρ(z) →
Wall Potential
14
12
10
8
6
4
2
0
150
100
50
0
−1.0
−2.0
−1.0
−0.5
0.0
0.5
1.0

F7

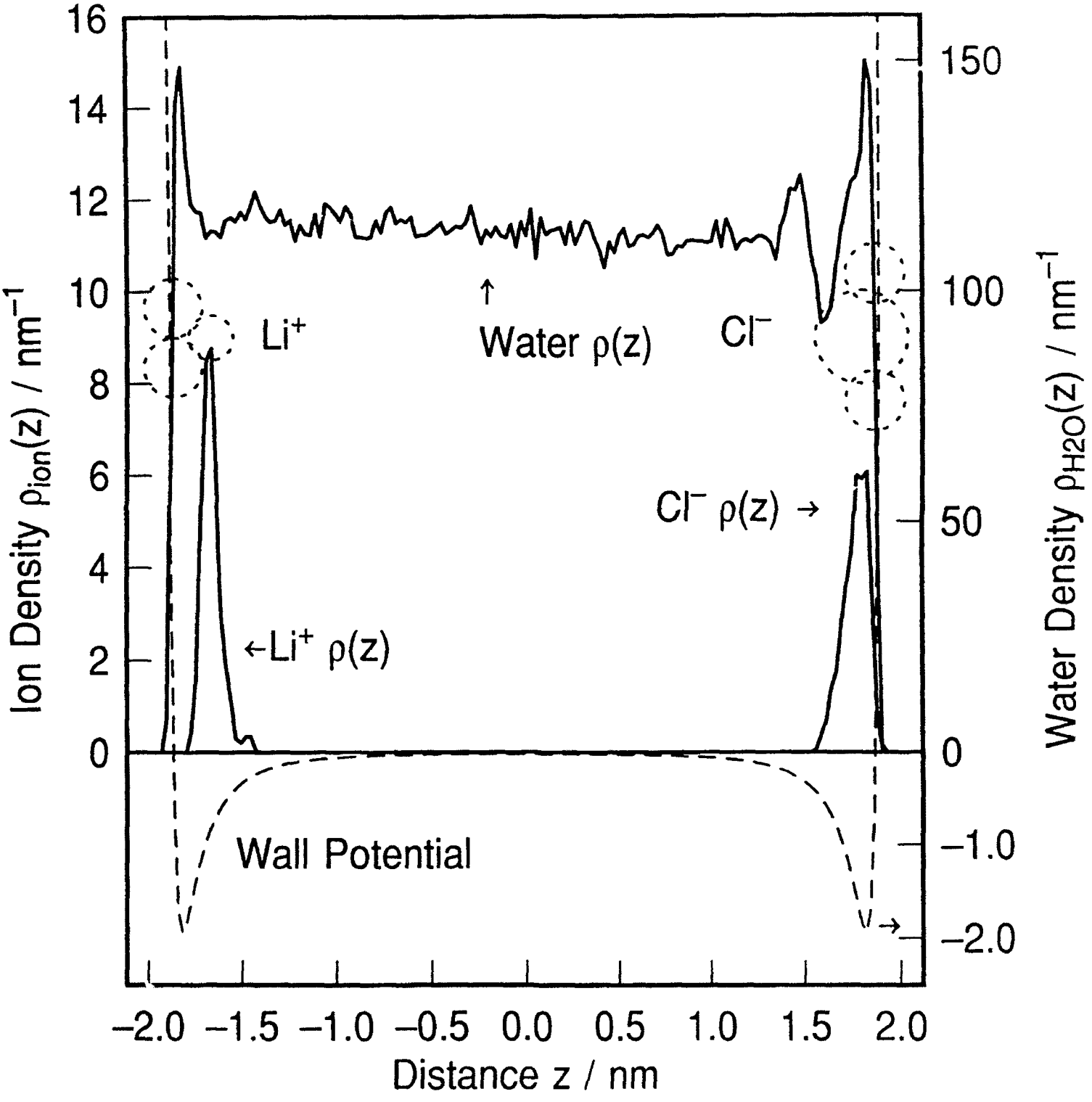
16
14
12
10
8
6
4
2
0
150
100
50
0
−1.0
−2.0
Ion Density $\rho_{ion}(z)$ / nm^{-1}
Water Density $\rho_{H2O}(z)$ / nm^{-1}
Li$^+$
Water ρ(z)
Cl$^-$
Cl$^-$ ρ(z) →
←Li$^+$ ρ(z)
Wall Potential
−2.0 −1.5 −1.0 −0.5 0.0 0.5 1.0 1.5 2.0
Distance z / nm

F8

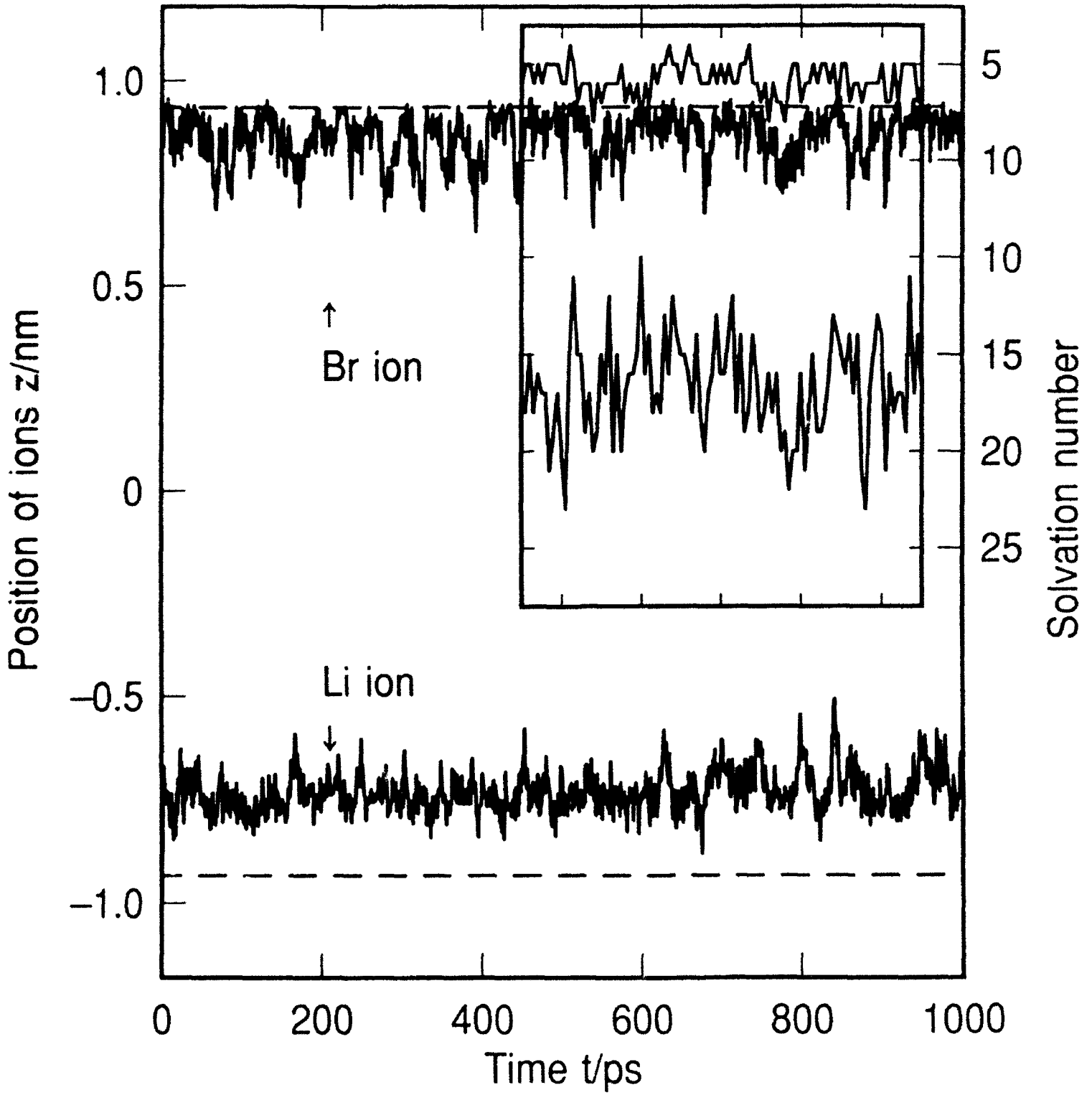
1.0
0.5
0
−0.5
−1.0
Position of ions z/nm
Br ion
Li ion
5
10
10
15
20
25
Solvation number
0
200
400
600
800
1000
Time t/ps

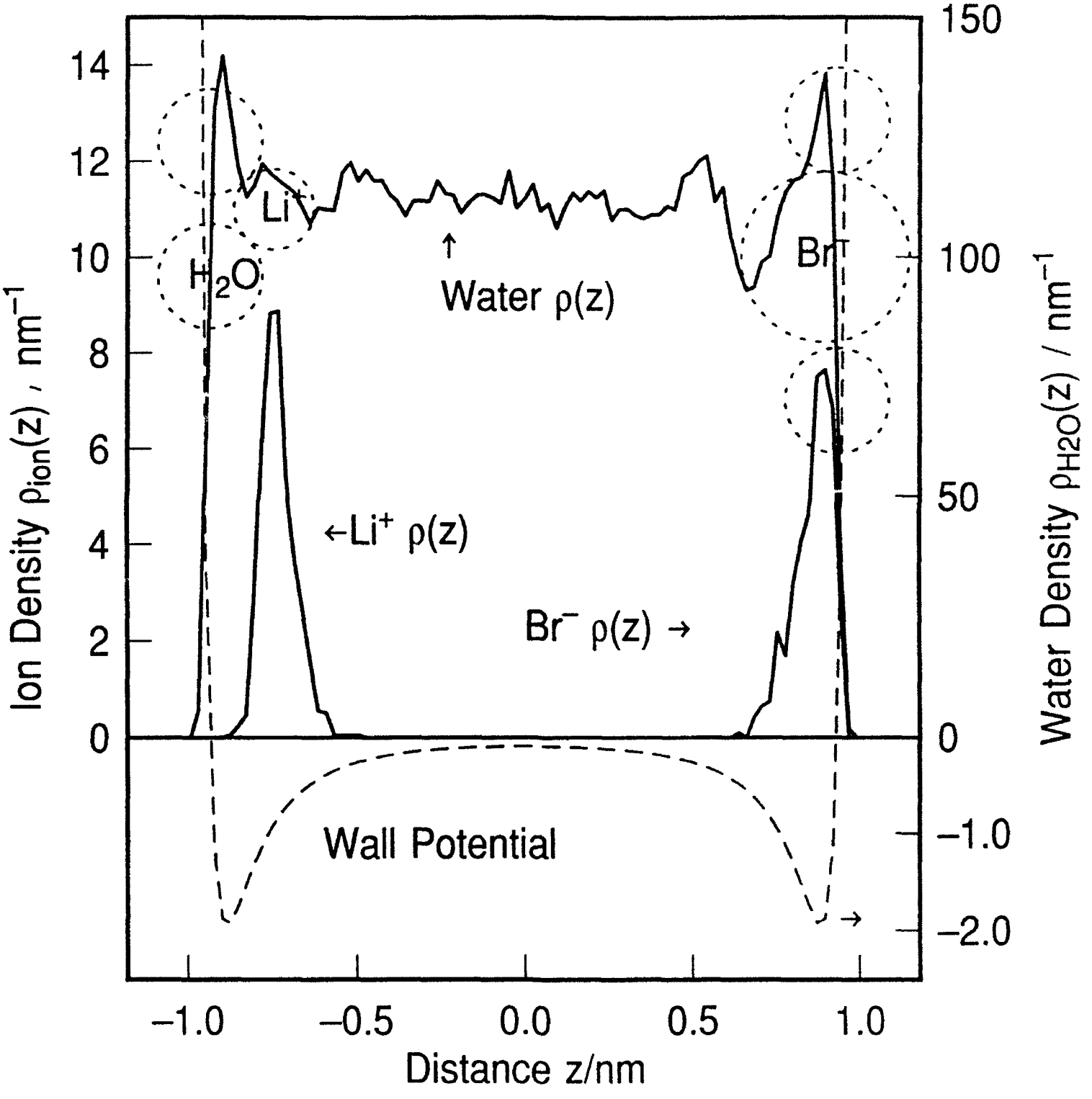
Ion Density $\rho_{ion}(z)$, nm^{-1}
Water Density $\rho_{H2O}(z)$ / nm^{-1}
Distance z/nm
Li
H_2O
Br
Water ρ(z)
←Li^+ ρ(z)
Br^- ρ(z) →
Wall Potential
14
12
10
8
6
4
2
0
150
100
50
0
−1.0
−2.0
−1.0
−0.5
0.0
0.5
1.0

F10

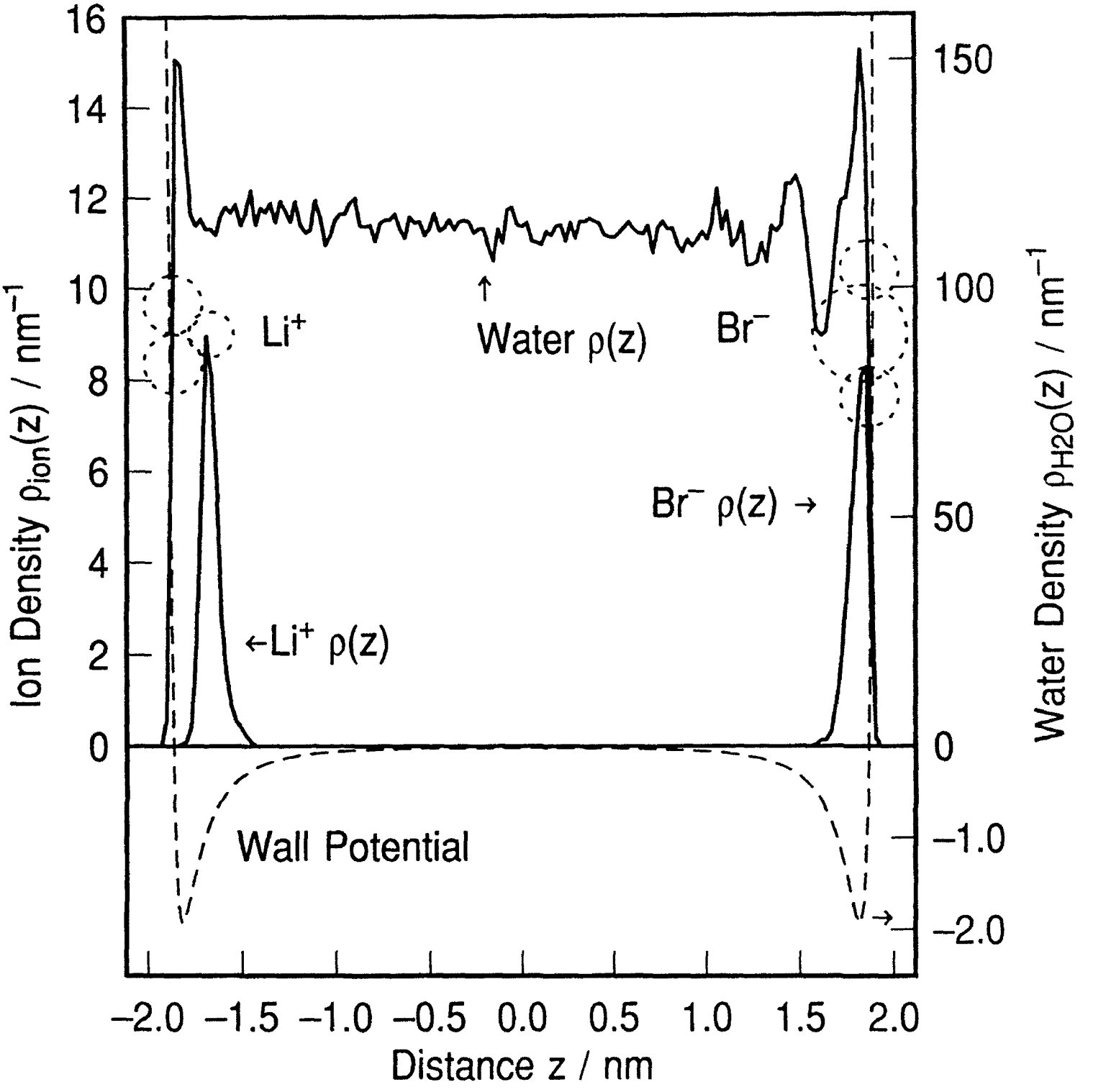
16
14
12
10
8
6
4
2
0
Ion Density $\rho_{ion}(z)$ / nm^{-1}
150
100
50
0
−1.0
−2.0
Water Density $\rho_{H2O}(z)$ / nm^{-1}
Li$^+$
Water ρ(z)
Br$^-$
Br$^-$ ρ(z) →
←Li$^+$ ρ(z)
Wall Potential
→
−2.0 −1.5 −1.0 −0.5 0.0 0.5 1.0 1.5 2.0
Distance z / nm

F11

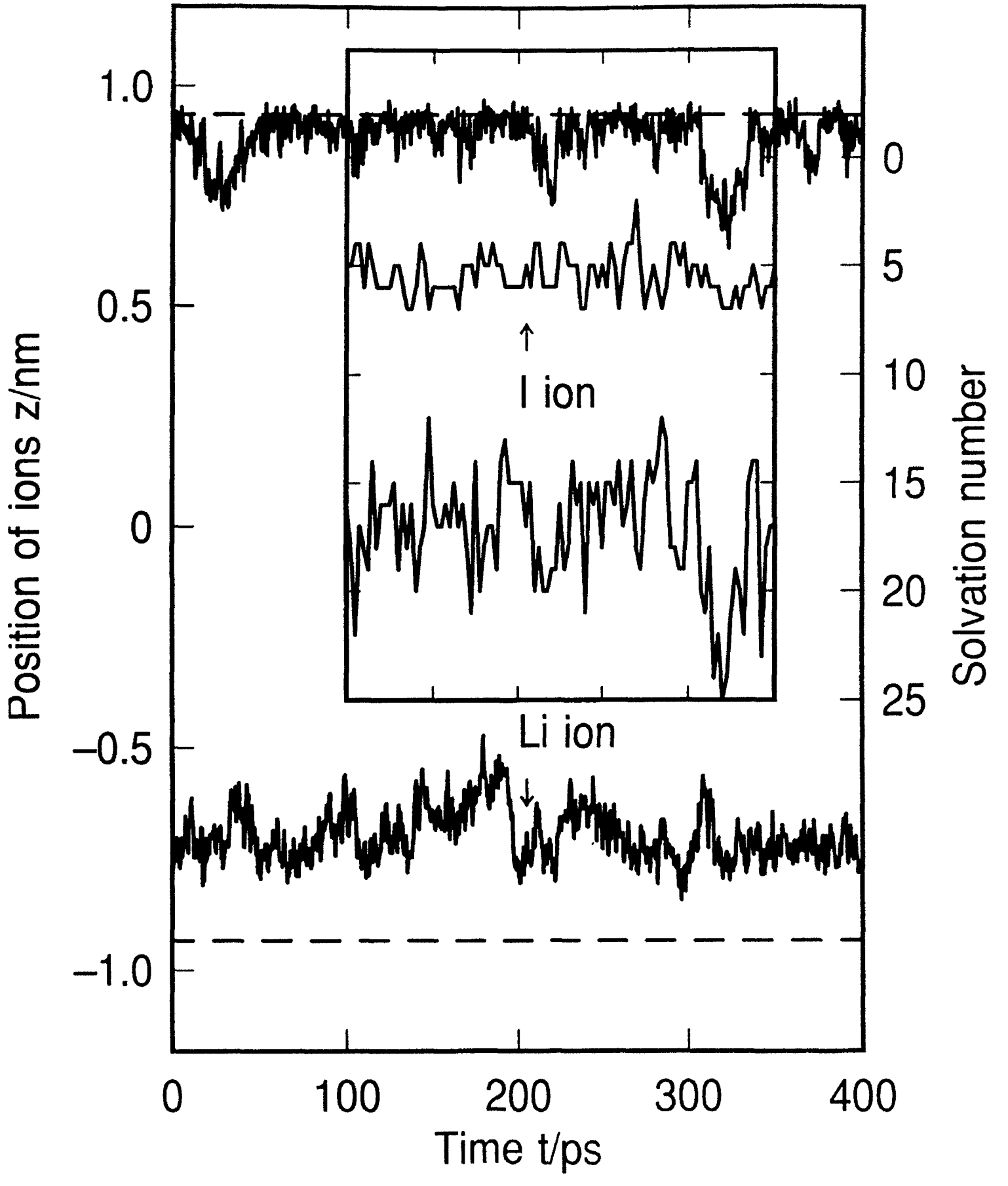
1.0
0.5
0
−0.5
−1.0
Position of ions z/nm
0
5
10
15
20
25
Solvation number
I ion
Li ion
0
100
200
300
400
Time t/ps

H12

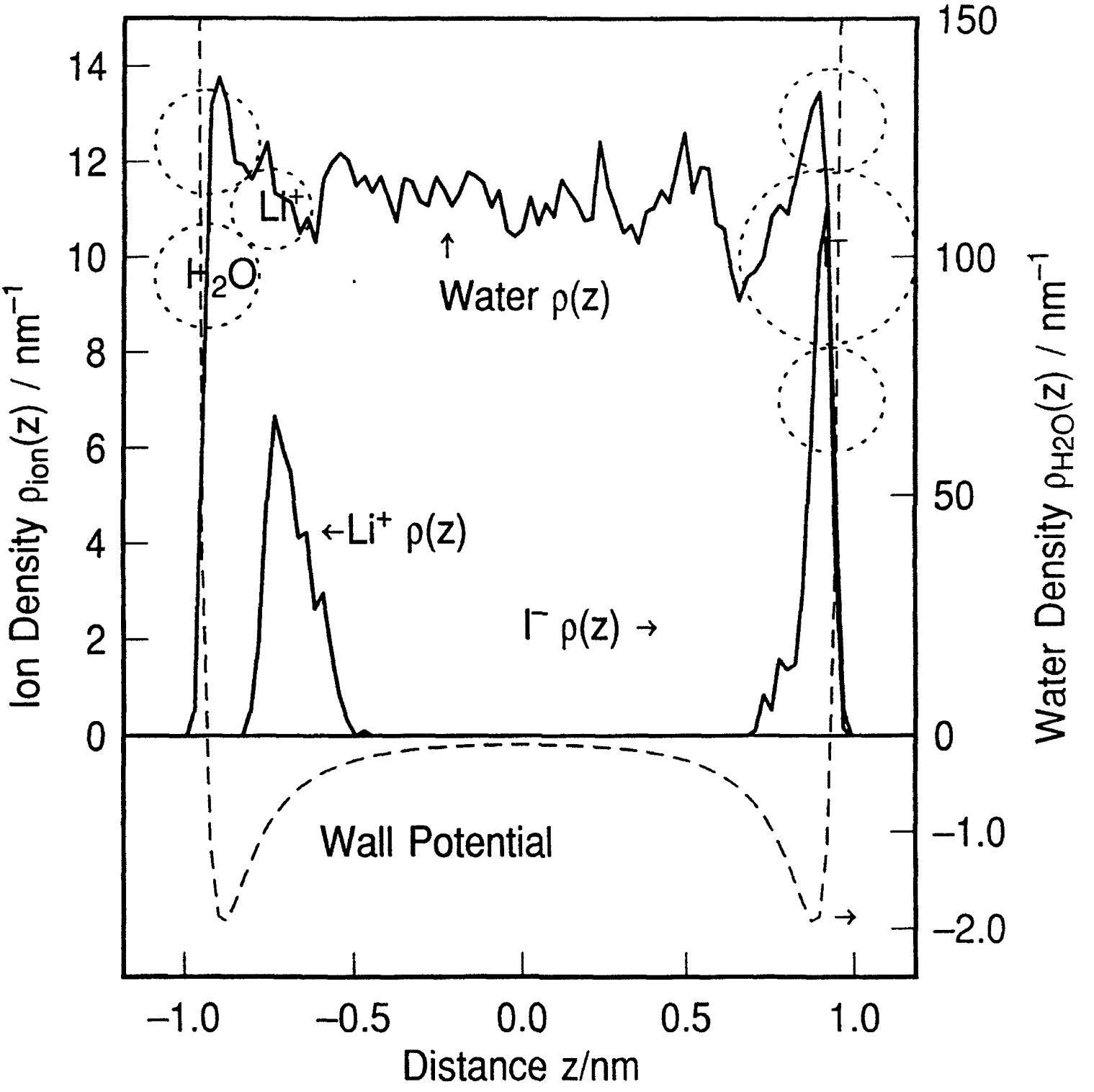
Ion Density $\rho_{ion}(z)$ / nm^{-1}
Water Density $\rho_{H2O}(z)$ / nm^{-1}
Distance z/nm
H_2O
Li^+
Water ρ(z)
←Li^+ ρ(z)
I^- ρ(z) →
Wall Potential
→
14
12
10
8
6
4
2
0
150
100
50
0
−1.0
−2.0
−1.0
−0.5
0.0
0.5
1.0

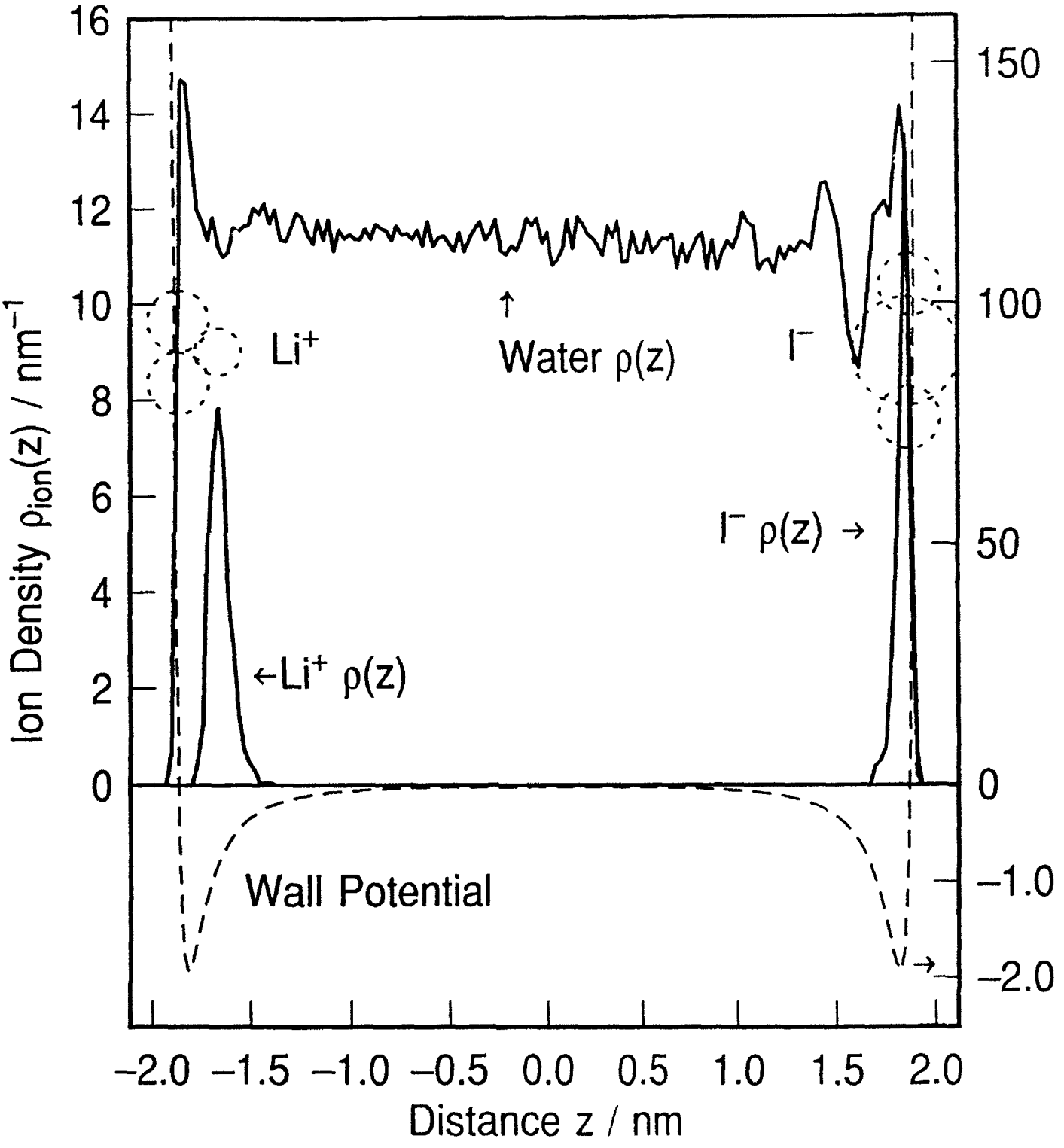
16
14
12
10
8
6
4
2
0
150
100
50
0
−1.0
−2.0
Ion Density $\rho_{ion}(z)$ / nm^{-1}
Li$^+$
Water ρ(z)
I$^-$
I$^-$ ρ(z) →
←Li$^+$ ρ(z)
Wall Potential
−2.0 −1.5 −1.0 −0.5 0.0 0.5 1.0 1.5 2.0
Distance z / nm